University of Alberta

The Effects of Biofilm on the Transport of Nanoscale Zerovalent Iron in the Subsurface

by

Robert N. Lerner

A thesis submitted to the Faculty of Graduate Studies and Research
in partial fulfillment of the requirements for the degree of

Master of Science

in

Environmental Science

Civil and Environmental Engineering

Spring 2011
Edmonton, Alberta

Examining Committee

Yang Liu, Civil and Environmental Engineering

Ania Ulrich, Civil and Environmental Engineering

Hongbo Zeng, Chemical and Materials Engineering

Dedication

For all the people who made this possible. Yes YOU.

Abstract

This study examines the effects of *Pseudomonas aeruginosa* (PAO1) biofilm, with a concentration of cells similar to that reported for saturated aquifers, on the transport of poly(acrylic acid) stabilized nanoscale zero valent iron (pnZVI) in 14 cm long, saturated, laboratory packed columns, with ionic strengths (ISs) of 1 and 25 mmol NaCl. With biofilm, the retention of pnZVI increased with higher solution IS, while IS played no role in the retention of nanoparticles without biofilm. However, the Tufenkji-Elimelech correlation equation predicts 5% less pnZVI collisions in biofilm coated columns due to a sixfold reduction of the Hamaker constant. Also, DLVO energy considerations predict the most favorable attachment for uncoated porous media at the higher IS. Reasons for the disagreement between theory and experiment are shown to be due to the non-ideality of the biofilm system. This research indicates that current laboratory studies underestimate nanoparticle transport distances in the subsurface.

Acknowledgements

I thank my supervisor, Dr. Yang Liu for her thoughtful guidance and assistance throughout my degree. Her knowledge is only surpassed by her kindness. Thanks also to Dr. Ania Ulrich for her help during my studies and for serving on my dissertation committee; and to Dr. Hongbo Zeng for being a dissertation committee member and for the kind use of his laboratory equipment.

These experiments would not have been possible without the help of various other professors and technicians. The expert advice and skills of Dr. Ming Chen with regards to preparing samples and capturing them in SEM and TEM images is greatly appreciated. Thanks to Dr. Jonathon Dennis from the department of Biological Sciences for the *Pseudomonas aeruginosa* (PAO1) bacteria. Thanks also to the laboratory technicians Jody Yu, Jela Burkus and Maria Demeter for their help and patience.

Thanks to my colleagues, Zhiya Sheng, Xuejiao Yang, Hamed Mahdavi, Peter Fayant, Geelsu Hwang, and Eun Sik Kim, who have provided me with immense help in understanding the day to day running of a laboratory, as well as in conducting my experiments.

I thank also my family and friends for their unwavering support. Without

the mental strength provided by my parents, aunt, brother (Jeremy David Lerner, best slum landlord ever), sister and girlfriend, I would never have even entered this program, let alone finished it. Thanks also to my friends for providing hours of distraction on the mountains, the trails, the rinks, the links and of course the ditches.

Table of Contents

List of Figures

List of Tables

List of Abbreviations

(AES) Auger electron spectroscopy

(CFT) colloid filtration theory

(CFU) colony forming unit

(CFU/gdw) colony forming units per gram of dry weight of soil

(CMC) carbox-ymethyl cellulose

(DLS) dynamic light scattering

(DLVO) Derjaguin-Landau-Verwey-Overbeek

(EDL) electrical double layer

(EPS) extracellular polymeric substances

(FWHM) full width at half maximum

(IS) ionic strength

(LB) Luria Burtani

(Na-PAA) sodium poly(acrylic acid)

(nZVI) nanoscale zerovalent iron

(PAA) poly(acrylic acid)

(PALS) phase analysis light scattering

(PCB) polychlorinated biphenyl

(pnZVI) poly(acrylic acid) stabilized nanoscale zero valent iron

(PV) pore volume

(SEM) scanning electron microscope

(SGW) simulated ground water

(snZVI) stabilized nanoscale zero valent iron

(TCE) trichloroethane

(TCLP) Toxicity Characteristic Leaching Procedure

(TD) thermal desorption

(TEM) transmission electron microscope

(WET) Waste Extraction Test

(XPS) X-ray photoelectron spectroscopy

(ZVI) zerovalent iron

List of Symbols

English

A_{11}, Hamaker constant of particle (J)

A_{123}, system Hamaker constant (J)

A_{22}, Hamaker constant of collector (J)

A_{33}, Hamaker constant of water (J)

A_s, specific surface area (m^2/g)

A_S, porosity dependent function

C/C_0, ratio of influent and effluent particle concentrations

D, diffusion constant

D_∞, diffusion coefficient

d_c, collector diameter (m)

d_p, particle diameter (m)

e, electron charge (C)

E, electric field

E_b, binding energy (J)

E_B, binding energy of replacement electron (J)

E_C, binding energy of ejected electron (J)

E_{core}, binding energy of core electron (J)

E_k, kinetic energy of electron (J)

E_p, photon energy (J)

f, porosity

g, acceleration due to gravity (m/s^2)

h, distance between two spheres (m)

k, rate constant $1/(M\ m^2\ s)$

k_b, Boltzmann constant

k_d, particle deposition rate coefficient

L, column length (m)

[Me], metal concentration (g/M)

M_i, molar concentration of electrolyte (mmol/L)

N_A, attraction number

N_{Av}, Avogadro's number (molecules/mole)

N_G, gravity number

N_{Pe}, Peclet number

N_R, aspect ratio

N_{vdW}, van der Waals number

r_c, collector radius (m)

R_h, hydrodynamic radius (m)

r_p, particle radius (m)

T, temperature (K)

U, fluid approach velocity (m/s)

v, reaction rate (s)

v_p, particle velocity (m/s)

z, electrolyte valence

Greek

α empirical attachment efficiency

γ, porosity function

δ, work function (J)

ϵ, relative permittivity

ϵ_0, permittivity in a vacuum (F/m)

η actual single collector removal efficiency

η_0, single collector contact efficiency

κ, inverse of double layer thickness (1/m)

λ, filter coefficient

λ_c, characteristic wavelength (m)

μ, fluid viscosity of medium (Pa s)

ρ_f, fluid density (kg/m^3)

ρ_p, particle density (kg/m^3)

ϕ, zeta potential (V)

ϕ_c, zeta potential of collector (V)

Φ_{el}, electrostatic energy (J)

ϕ_p, zeta potential of particle (V)

Φ_{total}, total DLVO interaction energy (J)

Φ_{vdW}, van der Waals energy (J)

Chapter 1

Introduction

1.1 Overview

Nanotechnology is at the forefront of the recent advances in materials technology. With sizes of less than 100 nm, nanoparticles have uniquely large surface area to volume ratios, and are thus highly reactive. Recently, there have been many studies regarding the cost effective in-situ remediation of otherwise difficult contaminants by using iron nanoparticles. Due to the high reactivity of these particles, their transport to the contamination zone can be difficult. However, by using surface modifications, many methods for increasing their mobility have been recently proposed.

Modeling the effects of various surface modifications on the transport of these nanoparticles is a very important aspect of current research. However, the transport effects of the abundant, naturally occurring microbiological populations found in the subsurface have been largely ignored, and will be the topic of this dissertation.

1.2 Objectives

The objective of these experiments is to better understand the effects of microbial populations on the transport of commercially available, stabilized zerovalent iron nanoparticles. Specifically, the objectives are to:

- Experimentally verify the surface coating used on commercially available stabilized zerovalent iron nanoparticles.
- Examine the effects of bacteria on the transport of these nanoparticles.
- Compare the measured transport characteristics to those predicted by commonly used theories.
- Suggest reasons for any discrepancies between predicted and measured transport.

1.3 Organization of the Dissertation

Following this introduction, Chapter 2 will provide a summary of common theories and recent publications on the history of iron nanoparticle use for remediation, discuss microorganisms and their formation and prevalence in the environment, and introduce common colloid filtration models and an interaction energy model that have been used to help interpret filtration results.

Chapter 3 will introduce the various laboratory equipment used, and briefly describe the theories and mechanisms by which they work. The materials used and their characterizations will also be introduced, as will the filtration and energy models used.

In Chapter 4 the results of the characterizations and models will be presented, and will be discussed individually. Chapter 5 will be a discussion about the interpretation of the collective results. Finally, Chapter 6 will focus on the implications of this experiment, and suggest future directions for research.

Chapter 2

Literature Review

2.1 Nanoparticles

Due to their special properties, specifically small size, and large surface area per unit mass, nanoparticles have been recently exploited for a wide array of applications. Consumer products using the term "nanotechnology" in their marketing include stain resistant clothing, transparent sunscreens, paints, sports equipment, and self cleaning glass, among many others (Doyle, 2006). Table 2.1, adapted from Nyer and Vance (2001), shows how rapidly the decrease in size of a smooth spherical particle effects the surface area per mass.

2.2 Environmental Application of Nanoparticles

Environmental applications of nanotechnology have recently been exploited in the field of contaminant remediation, with ongoing research readily confirm-

Table 2.1: The resulting surface area per mass of a spherical particle based on the diameter.

Diameter	Surface Area (m^2/g)
100 microns	0.00076
10 microns	0.076
1 micron	0.76
100 nanometers	7.6
50 nanometers	15.3
10 nanometers	76.3

ing new remediation potential of a variety of nanoparticles (Amir and Lee, 2011; Ambashta and Sillanpaa, 2011; Kanel *et al.*, 2011). However, due to the well developed science surrounding millimeter scale zerovalent iron (ZVI) remediation technologies (e.x. Cantrell *et al.*, 1995; Puls *et al.*, 1999; Su and Puls, 2003), the specific use of nanoscale ZVI (nZVI) is the most widespread (Zhang, 2003).

2.3 Nanoscale Zerovalent Iron

Research into the use of ZVI for environmental remediation purposes has been ongoing since Gillham and O'Hannesin (1994) demonstrated its applicability for the in-situ degradation of halogenated methanes, ethanes and ethenes. That study, as well as subsequent investigations, have revealed that degradation rates tend to improve with an increase in the available surface area of iron per volume of treatment solution (Ponder *et al.*, 2000; Wang and Zhang, 1997). These studies further directed research into investigating the use of nZVI for in-situ immobilization of heavy metals (Xu and Zhao, 2007), degra-

dation of trichloroethene (TCE) and polychlorinated biphenyls (PCBs) (Wang and Zhang, 1997) as well as the reduction of many other compounds, as shown in the non-exhaustive list in Table 2.2, adapted from Zhang (2003).

Table 2.2: Some common environmental contaminants that can be transformed by nanoscale iron particles.

Chlorinated methanes	Trihalomethanes
Carbon tetrachloride	Bromoform
Chloroform	Dibromochloromethane
Dichloromethane	Dichlorobromomethane
Chloromethane	Chlorinated ethenes
Chlorinated benzenes	Tetrachloroethene
Hexachlorobenzene	Trichloroethene
Pentachlorobenzene	*cis*-Dichloroethene
Tetrachlorobenzenes	*trans*-Dichloroethene
Trichlorobenzenes	1,1-Dichloroethene
Dichlorobenzenes	Vinyl chloride
Chlorobenzene	Other polychlorinated hydrocarbons
Pesticides	PCBs
DDT	Dioxins
Lindane	Pentachlorophenol
Organic dyes	Other organic contaminants
Orange II	N-nitrosodimethylamine
Chrysoidine	TNT
Tropaeolin O	Inorganic anions
Acid Orange	Dichromate
Acid Red	Arsenic
Heavy metal ions	Perchlorate
Mercury (II)	Nitrate
Nickel (II)	
Silver (I)	
Cadmium (II)	

2.3.1 Remediation of Specific Contaminants

A small sample of the research and mechanisms by which nZVI has been used for the remediation of sites contaminated by chromium and halogenated

compounds is presented.

Chromium

The U.S. EPA (1998a) classifies hexavalent chromium [chromium (VI)] as a toxic substance. Oral ulcers, diarrhea, abdominal pain, indigestion, vomiting, leukocytosis, and the presence of immature neutrophils are some of the negative health effects seen after consumption of this compound in high doses (Zhang and Li, 1987). Leaching of chromium into drinking water is the major exposure pathway for humans. Thus, reducing the mobility of this metal in contaminated soils is viewed as an effective remediation tool (Czupyrna *et al.*, 1992). Previously, studies have focused on adding immobilizing chemicals to soil such as synthetic zeolites, like crystalline alumino silicates (Oste *et al.*, 2002). Studies have also shown that chromium (VI) can be reduced to the less mobile, and less toxic chromium (III) form (U.S. EPA, 1998b) by iron (II) oxidation (Seaman *et al.*, 1999).

More recently, research has been done using zerovalent iron to reduce chromium (VI) to chromium (III) via Equation (2.1), and ultimately forming precipitates via Equations (2.2) and (2.3) (Lo *et al.*, 2006).

$$CrO_4^{2-} + Fe^0 + 4H_2O_{(l)} \longleftrightarrow Cr^{3+} + Fe^{3+} + 8OH^- \tag{2.1}$$

$$(1-x)Fe^{3+} + xCr^{3+} + 3H_2O_{(l)} \longleftrightarrow (Cr_xFe_{1-x})(OH^-)_{3(s)} + 3H^+ \tag{2.2}$$

$$(1-x)Fe^{3+} + xCr^{3+} + 2H_2O_{(l)} \longleftrightarrow Cr_xFe_{1-x}OOH_{(s)} + 3H^+ \qquad (2.3)$$

The applicability of nanosized particles for chromium reduction by zerovalent iron is best described through the kinetics shown in Equation (2.4) (Ponder *et al.*, 2000).

$$v = kA_s[Me] \qquad (2.4)$$

Here, v is the reaction rate, k is the rate constant, A_s is the specific surface area of the iron and [Me] is the metal concentration. From the above equation, it is clear that smaller particles, having larger specific surface areas (see Table 2.1), greatly increase the rate of reaction. Utilizing this increase in reactivity, current research into chromium remediation using ZVI is being conducted with nanosized particles.

Many studies have thus far quantified the capacity of nZVI to reduce chromium (VI). In a study conducted by Li *et al.* (2008), wastewater samples were obtained from a Newark, New Jersey chromium ore process residue site, containing a chromium (VI) concentration of 10 900 μg/L. Batch experiments were conducted using concentrations of nZVI ranging from 0.25 to 25 g/L for reduction of hexavalent chromium to the less toxic form of trivalent chromium. The nZVI exhibited a reduction capacity of up to 180 mg Cr/g nZVI, or 50 – 70 times that of microscale iron (Cao and Zhang, 2006).

The above results have lead the way for further investigation into the poten-

tial of both in situ and ex situ nZVI applications. Xu and Zhao (2007) were one of the first to investigate the use of carboxy-methyl cellulose (CMC) supported nZVI (He *et al.*, 2007) for in situ reductive immobilization of chromium (VI) in sandy loam soil. The effectiveness of the CMC-supported nZVI on immobilizing the chromium was measured by the Toxicity Characteristic Leaching Procedure (TCLP; U.S. EPA, 2003) and the California Waste Extraction Test (WET; State of California, 2005). The TCLP and WET tests indicated total chromium elution reductions of 90 % and 76 %, respectively. Also, the eluted chromium was all in the form of the less toxic chromium (III).

Another experiment, by Franco *et al.* (2009), used a packed bed column reactor to test stabilized (with CMC) nZVI on the removal of chromium (VI) from contaminated soil. The soil used was "frank clay sandy texture" from a Brazilian industrial waste landfill, with a contamination of 456±35 mg/kg chromium (VI). From a column reactor test, treated with simulated ground water (SGW), and a 1:4 and 1:8 molar ratio of [Cr(VI)]:[nZVI], results indicated that in order to bring the Cr(VI) concentrations down to the 0.05 mg/L Brazil regulated level for total chromium, approximately 3.0 and 1.5 pore volumes (PVs) were needed for the 1:4 and 1:8 [Cr(VI)]:[nZVI] molar ratios, respectively. In comparison, greater than 35 PVs of the SGW were needed to achieve this reduced concentration.

Halogenated Compounds

Historically, treating non-volatile halogenated organic compounds has been a costly, ex-situ process. For example, applicable treatment technologies for

PCBs include excavation and treatment via soil washing, thermal desorption (TD), or solvent extraction (Lowry and Johnson, 2004). The costs associated with treating this type of contamination are clearly illustrated by the approximate half a billion dollar estimate (not including capital costs) placed on drudging and treating the 2.7 million cubic yards of sediment contaminated by PCBs in the Upper Hudson River (U.S. EPA, 2000).

Research into dehalogenation of halogenated compounds using iron has been underway for years. The reaction between ZVI and chlorinated compounds is described by Equation (2.5) (Zhang *et al.*, 1998). As one of the first examples, Senzaki and Kumagai (1988, 1989) showed via column and batch reactors that TCE and 1, 1, 2, 2-Tetrachloroethane could be effectively treated with iron powders. Subsequently, Senzaki (1991) discovered that the surface area of the iron appeared to have the biggest impact on the reaction rate.

$$C_xH_yCl_z + zH^+ + zFe^0 \longleftrightarrow C_xH_{y+z} + zFe^{2+} + zCl^- \tag{2.5}$$

Another study, by Satapanajaru *et al.* (2008), examined the use of ZVI, and nZVI on the dechlorination of atrazine (2-chloro-4ethylamino-6-iso-propylamino-1,3,5-triazine) in soil. They spiked Marb Bon Series soil from eastern Thailand with atrazine to get a concentration of 20 mg atrazine per kg of soil. The samples were composed of 2 g of either ZVI or nZVI, with 20 g of the contaminated soil. The nZVI treated soil showed an atrazine removal efficiency of 52±8 %, substantially higher than the 20±11 % removal efficiency measured for the larger ZVI.

The applicability of adding nZVI to existing ex situ soil treatments has also been extensively studied. For example, TD is a common process used for treating PCBs (Norris *et al.*, 1999). Due to the high temperatures needed, Varanasi *et al.* (2007) looked at the effects of adding nZVI into the TD process in order to make it more economical. They first found that mixing PCB contaminated soils with nZVI at room temperatures did not cause a significant amount of PCB destruction. This was likely due to the slow transfer of PCBs from the soil to the iron surface. However, by adding nZVI to the contaminated soil before TD (the most cost effective ratio was found to be 0.1 g nZVI per 10 g soil), the required temperatures at which this process was successful at dechlorinating the PCBs to biphenyl was lowered from approximately 800°C to 300°C.

2.4 nZVI Transport

Although vast gains in degradation rates of a plethora of contaminants were realized through the higher surface area, and hence reactivity of nZVI (Cao and Zhang, 2006; Wang and Zhang, 1997), the new problem that needed to be addressed by researchers was the reduction in transport distances, due to their tendency to agglomerate (Schrick *et al.*, 2004). Several different methods have been proposed to increase transport distances while maintaining reactivity, enabling the nZVI injections to penetrate into contaminated zones, thereby allowing for efficient degradation. Starch (He and Zhao, 2005), sodium-CMC (He *et al.*, 2007), poly(acrylic acid) (PAA) (Schrick *et al.*, 2004), hydrophilic

carbon (Schrick *et al.*, 2004), polyoxyethylene sorbitan monolaurate (Kanel *et al.*, 2007), cetylpyridinium chloride (Chen *et al.*, 2004), PolyFlo resin Ferragels (Ponder *et al.*, 2000), oil/surfactant mixtures (Quinn *et al.*, 2005) and others have been used to stabilize or support nZVI, with variable effects on their reactivity (Saleh *et al.*, 2007).

2.4.1 Transport Models

In order to help explain, and therefore predict the transport of various versions of stabilized nZVI (snZVI) in saturated subsurface environments, authors have relied upon classical colloid filtration theory (CFT). The specifics of CFT, as well as the current form most commonly used for modeling transport through saturated porous media, will be introduced in the following sections followed by a brief summary of some recent studies utilizing this theory.

Beginnings of Colloid Filtration Theory

The theory of colloid filtration was first introduced by Yao *et al.* (1971) whereby the transport mechanism of smaller particles was determined to be through Brownian motion (diffusion), and the transport of larger particles was ascertained to be governed by interception and settling. This work was further developed by Rajagopalan and Tien (1976), this time utilizing the Happel sphere in cell model (Happel, 1958), whereby the porous media is assumed to be a collection of identical spheres surrounded by a frictionless fluid. The major advance of Rajagopalan and Tien (1976) was to propose a closed form expression for single collector efficiency (R-T model).

Current CFT Model

More recently, Tufenkji and Elimelech (2004a) noted that the R-T model broke down in most environmentally relevant conditions due to the omission of van der Waals and hydrodynamic interactions for small particles filtered in the diffusion dominated regime. These authors developed a new closed form expression for single collector contact efficiency (η_0), the T-E model, based on rigorous regression analysis of numerical solutions of the convection diffusion equation and an assumption of additivity of particle deposition due to diffusion, interception and gravity shown as respective dimensionless terms in Equation (2.6) (Tufenkji and Elimelech, 2004a). Each component of Equation (2.6) is expanded in Equations (3.5) to (3.10) in Chapter 3.

$$\eta_0 = 2.4A_S^{1/3}N_R^{-0.081}N_{Pe}^{-0.715}N_{vdW}^{0.052} + 0.55A_S N_R^{1.675}N_A^{0.125} + 0.22N_R^{-0.24}N_G^{1.11}N_{vdW}^{0.053} \tag{2.6}$$

The T-E equation has been found to be in agreement with previous data for which electrical double layer (EDL) interactions were not significant. The published data covered an array of different particle sizes (0.1 to 4 μm), collector diameters, and approach velocities for latex particles using glass beads as collectors (Tufenkji and Elimelech, 2004a). The equation has also been repeatedly used in the literature for a variety of 50 nm particles (Schrick *et al.*, 2004; Hydutsky *et al.*, 2007; Pelley and Tufenkji, 2008). However, a commonality of CFTs, including the T-E equation, is their inability to predict colloid removal rates in environmentally relevant systems, due to unfavorable repulsive condi-

tions related to the particle and collector surface charge, and possibly other, less well understood phenomena such as steric forces (Saleh *et al.*, 2008). Thus, the actual single collector removal efficiency [η, Equation (2.7)] for a particular setup can be found through laboratory scale column tests by finding an empirical attachment efficiency [α, Equation (2.8)] using parameters of collector diameter (d_c), porosity (f), column length (L), and ratio of influent and effluent particle concentrations (C/C_0). Finally, the particle deposition rate coefficient [k_d, Equation (2.9)] and filter coefficient [λ, Equation (2.10)] are measures of filtration, utilizing calculated and measured values of η_0 and α, and the fluid approach velocity (U), that are commonly used in transport studies.

$$\eta = \alpha\eta_0 \tag{2.7}$$

$$\alpha = -\frac{2}{3}\frac{d_c}{(1-f)L\eta_0}ln(C/C_0) \tag{2.8}$$

$$k_d = \frac{3}{2}\frac{(1-f)}{d_c f}U\alpha\eta_0 \tag{2.9}$$

$$\lambda = -\frac{3}{2}\frac{(1-f)}{d_c}\alpha\eta_0 \tag{2.10}$$

2.4.2 Particle–Collector Interaction Model

Derjaguin-Landau-Verwey-Overbeek (DLVO) Model

It has been reported that CFT breaks down in the presence of repulsive Derjaguin-Landau-Verwey-Overbeek (DLVO) (Derjaguin and Landau, 1941; Verwey, 1947) forces (e.x. Saleh *et al.*, 2008). DLVO theory proposes that the interaction of two bodies is governed by the summation of electrostatic (repulsive or attractive) and universal van der Waals (attractive) forces. The governing relations are shown and described in Equations (3.11) to (3.14) and Table 3.2 in Chapter 3.

Tufenkji and Elimelech (2005) showed that using DLVO energy profiles (an example can be seen in Figure 4.7 in Chapter 4), a repulsive barrier to particle deposition is seen at all but very high ionic strengths (ISs). Those authors also showed that there exists, at lower IS, a secondary energy minimum at a distance greater than the repulsive barrier. Particles overcoming the energy barrier and those getting stuck in the secondary energy minimum are said to attach to the collector via "slow" and "fast" deposition, respectively (Tufenkji and Elimelech, 2004b). The DLVO energy profiles of larger particles tend to show higher energy barriers, as well as deeper secondary minima when compared to smaller ones.

Under some circumstances, research has shown that deposition of colloids in secondary energy minima could explain deviations from CFT (Tufenkji and Elimelech, 2005; Redman *et al.*, 2004) for latex particles as small as 63 nm. DLVO energy considerations will be used when interpreting data from this

experiment.

2.4.3 Current Research Utilizing CFT

In order to discuss the application of transport results from laboratory tests to the real subsurface, several authors have relied on CFT. Saleh *et al.* (2008), determined the relative abilities of different stabilizers (poly(methacrylic acid)-b-(methyl methacrylate)-b-(styrene sulfonate) triblock copolymer, polyaspartate biopolymer and sodium dodecyl benzene sulfonate surfactant) to improve transport of nZVI, while He *et al.* (2009) examined the use of CMC as a stabilizer for nZVI. Both of these studies, using predictions of η_0 from the T-E model, and experimentally determined values of α, found the filtration lengths needed to remove 99% of the modified particles by rearranging Equation (2.8). Caveats regarding the actual application of these filtration lengths to field applications were discussed by Saleh *et al.* (2008) regarding unconsolidated aquifers, variations in injection velocities and the higher nZVI concentrations typically used for remediation.

Another study, conducted by Kanel *et al.* (2007) investigated, among other parameters, the transport of non-ionic surfactant Tween 20 (polyoxyethylene sorbitan monolaurate) modified nZVI through various porous media. This study again used predictions of η_0 from the T-E model, as well as elution experiments to obtain experimental values of α which were subsequently compared to α values from other studies.

Lastly, Schrick *et al.* (2004) investigated the transport effects of anionic hydrophilic carbon and PAA supported nZVI on various soils through elu-

tion tests. Utilizing the eluted values of nZVI, in conjunction with η_0 values predicted from the T-E model and Equation (2.10), filtration lengths were determined, with caution urged due to the inhomogeneity of collector grain sizes in natural systems.

2.5 Microbial Populations in the Subsurface

One similarity between the previous nZVI transport studies is their inattention to the biological aspect of the soil matrix. For example, in-situ bioremediation, a remediation technology whose use was first documented in the 1970's (Pardieck *et al.*, 1992), relies on the use of microorganisms naturally occurring in the contaminated soils.

2.5.1 Microbial Prevalence

Studies have estimated the number of viable bacterial cells in various saturated aquifers to be on the order of 10^6 to 10^7 colony forming units (CFUs) per gram of dry weight of soil (CFU/gdw) (Balkwill and Ghiorse, 1985; Bone and Balkwill, 1988; Wilson *et al.*, 1983; Webster *et al.*, 1985). However, in nearly all natural systems, bacteria are not present as single (planktonic) cells, but rather as microbial communities in a biofilm (Watnick and Kolter, 2000).

2.5.2 Biofilm

Biofilm is a complex aggregation of bacterial cells and secreted extracellular polymeric substances (EPS) that provides advantageous living conditions to

the bacteria. Inside of a biofilm, bacteria have been shown to acquire an increased resistance to toxic substances (Costerton *et al.*, 1987), potentially due to the protective EPS layer, or the rapid intercellular exchange of genetic materials occurring within the biofilm (Watnick and Kolter, 2000). In natural systems, biofilms are usually formed as an aggregate of bacterial species, and have complex, heterogeneous structure (Costerton *et al.*, 1999). Biofilms have even been likened to the tissues of higher organisms due to their complex structure (Costerton *et al.*, 1995).

2.5.3 Biofilm Formation

Biofilm growth patterns have been shown to be highly variable and dependent on environmental conditions including available bacteria, flow rate, nutrient availability, pH, temperature and others (Hall-Stoodley and Stoodley, 2005). Thus, every natural system will have its own unique biofilm properties. It is generally believed that surfaces with increased roughness and hydrophobicity will form biofilm more quickly. However, in aquatic systems, the surface will become covered with a conditioning film composed mainly of proteins present in the environment, therefore governing the interactions with bacteria (Donlan, 2001). The bacterial surface composition also plays an important role in the initial attachment, with properties such as the presence of flagella (Korber *et al.*, 1989) and fimbrea (Rosenberg *et al.*, 1982), as well as surface hydrophobicity (Waldvogel and Bisno, 2000) affecting attachment. The basic principle of biofilm formation, illustrated in Figure 2.1, is thought to follow the following steps:

1. Initial attachment to surface

2. Irreversible attachment to surface

3. Micro-colony formation

4. Macro-colony formation

5. Release of planktonic cells

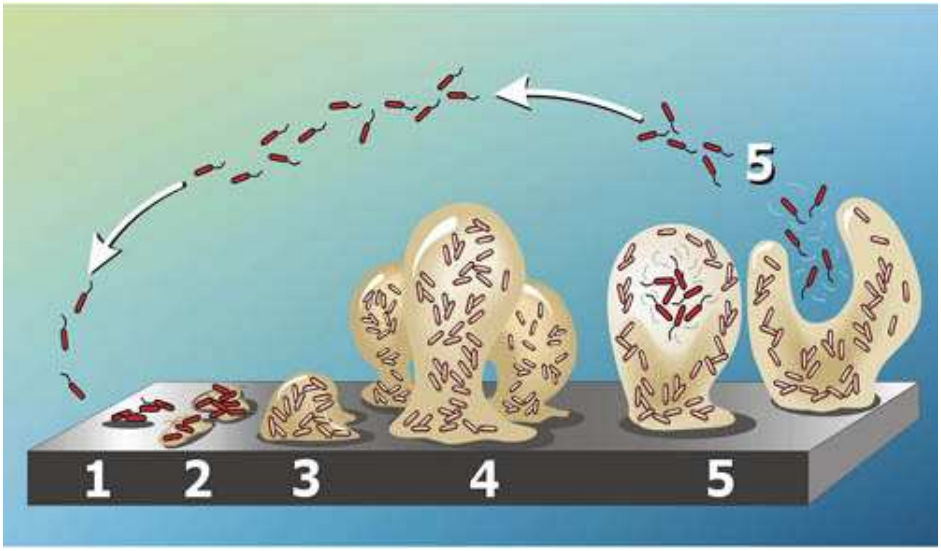

Figure 2.1: The steps of biofilm development. Courtesy, Montana State University Center for Biofilm Engineering, P Dirckx.

2.5.4 Extracellular Polymeric Substances

EPS is a combination of carbohydrates, proteins, lipids, nucleic acids and various heteropolymers that are secreted by bacterial cells (Christensen, 1989). These secretions, along with the bacterial cells, make up the protective layer that is biofilm. EPS production and composition is highly varied between

different bacteria, and even different strains of the same bacteria. For example, the EPS of *Pseudomonas aeruginosa* strain PAO1 (used in this study) is mainly composed of carbohydrates, while strain PDO300 excretes EPS consisting of mainly uronic acid (Liu and Li, 2008). The main purpose of EPS is not solely for protection from outside factors, but can also be used as a substrate for bacterial growth in nutrient deficient conditions, as shown by Zhang and Bishop (2003) for the native EPS producers, as well as other bacteria.

2.5.5 *Pseudomonas aeruginosa* (PAO1)

P. aeruginosa is a rod shaped, Gram-negative bacteria, measuring approximately 1.5μm by 0.5μm, that is readily found in natural aquatic systems, including marine habitats, plant tissues and soils (Hardalo and Edberg, 1997). This bacteria is regarded as a human pathogen and has been identified as a main culprit in burn infections and in the lungs of cystic fibrosis patients (Smith and Iglewski, 2003). *P. aeruginosa* is generally considered to be an aerobic respirator. However, biofilms of this bacteria have recently been shown to be able to grow and thrive in certain anaerobic conditions (Yoon *et al.*, 2002).

The PAO1 strain is the most common form of *P. aeruginosa* used in laboratory tests (Klockgether *et al.*, 2010). Due to the prevalence of this bacteria, current research interests range from its response to conditions occurring in spaceflight (Crabbe *et al.*, 2011) to environmental variables affecting its use in metal immobilization applications (Hunter *et al.*, 2010). Figure 2.2 shows a scanning electron microscope (SEM) image (Hitachi SEM S-2500), taken from this study, of *P. aeruginosa* (PAO1) bacterial cells, grown on glass beads and

enmeshed in a biofilm (information on the processing of this sample can be found in Chapter 3).

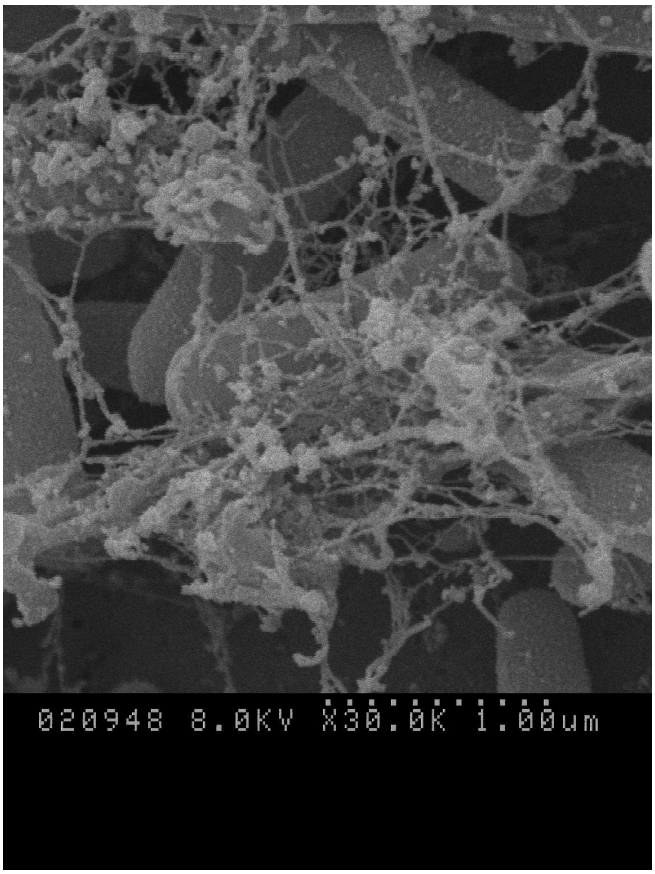

Figure 2.2: SEM image (Hitachi SEM S-2500) of *P. aeruginosa* bacterial cells enmeshed in biofilm from this study.

A possible explanation for the ubiquity of this bacteria in nature is its 6.3 million base pair genome (strain PAO1), with its length and complexity allowing for evolutionary adaptations that have enabled, among other things, increased resistance to antibiotics (Stover *et al.*, 2000). However, due to the breadth of its genome, research is also being conducted into the identification and exploitation of genes associated with increasing the bacterium's susceptibility to antibiotics (Chen *et al.*, 2010).

2.6 Knowledge Gap

The presence of biofilm in the real subsurface environment complicates the ideal situation of filtration modeled in CFT. At the time of writing, the authors know of only one other study that investigates the transport of engineered nanoparticles (C_{60}) through biofilm coated porous media (Tong *et al.*, 2010), with results indicating that DLVO forces did not accurately describe the findings. Due to the ongoing research into the use of snZVI for environmental remediation, as well as the dependence of that research on the use of CFT, the effects of biofilm on the transport characteristics of commercially available, PAA stabilized nZVI (pnZVI) is the focus of this current study. The analysis will attempt to explain the relative attachment efficiencies (α) obtained from the breakthrough curves of pnZVI injections, for both uncoated and biofilm coated saturated porous media, for solution ISs of 1 and 25 mmol NaCl.

In an attempt to explain the differences in observed pnZVI transport through biofilm coated porous media, DLVO energy considerations will also be used. We find that the presence of biofilm hinders the transport of pnZVI through saturated porous media, and these results are not predicted by the T-E model, or explained by DLVO energy considerations.

Chapter 3

Methodology

3.1 Materials

3.1.1 Chemicals and Reagents

For these experiments, all basic laboratory chemicals (HCl, NaOH etc.) were at least A.C.S. grade, and all water was ultra pure, from an Elga Maxima dispenser. Growth media was sterilized by autoclaving at 121°C for at least 15 minutes and allowed to cool prior to use. Reagents used for iron determination (hydroxylamine hydrochloride, 1-10 phenanthroline monohydrate) were A.C.S. grade from the Ricca Chemical company, while the ferrous ammonium sulfate, used for iron standardizing, was A.C.S. grade from Fisher Scientific.

3.1.2 Porous Media

The porous media used for these experiments was class V soda-lime glass spheres with a factory reported average diameter of 550 μm, from MO-Sci

Specialty Products L.L.C. The composition of these beads was reported to be ∼70% SiO_2, ∼15% Na_2O, ∼10% CaO, ∼3% Al_2O_3, ∼3% MgO and <0.3% Fe_2O_3 (Tufenkji and Elimelech, 2004b).

3.1.3 Nanoparticles

Commercially available (Kadar *et al.*, 2011), PAA stabilized (Klimkova *et al.*, 2011) nanoscale zerovalent iron particles with an Fe^0 core and Fe-oxide shell (Sarathy *et al.*, 2009), NANOFER 25S, were graciously provided as a sample from Nano Iron, S.R.O. (Czech Republic) and were delivered in 50 mL volumes of concentrated slurry. An analysis of the surface composition of these particles is included in Chapter 4.

Due to the high initial concentration of NANOFER 25S upon delivery, 4 mL were mixed with approximately 100 mL of ultra pure water (final concentration of ∼4 g/L) and allowed to stabilize for approximately three months at ∼4°C before the first column experiments were conducted with a dilution of the stably suspended iron in the supernatant. Due to the slight drop off of measured supernatant iron concentration over time, as well as the general tendency for pnZVI to oxidize and aggregate, all duplicate transport experiments, as well as characterizations, were completed within 5 days of each other. This short time frame allowed for consistency of zeta potential, size, and reactivity of the pnZVI.

Information on the transport experiments, as well as characterization, are described in detail later.

3.1.4 Bacterial Culture

Gram-negative *P. aeruginosa*, wild-type PAO1, was acquired from Dr. Jonathan Dennis from the department of Biological Sciences at the University of Alberta. Upon receipt, a single colony from the streaked plate was transferred to Luria Burtani (LB) Lennox broth, and shaken at 37°C and 200 rpm for ∼20 hours (to reach the stationary phase). 2 mL of the suspension was then added to 2 mL of glycerol and stored in the freezer at -80°C. When needed, the sample was thawed and streaked onto LB Miller Agar, then incubated overnight at 37°C. A single colony was then transferred to 450 mL of LB broth and shaken for ∼20 hours at 37°C and 200 rpm. The use of a single bacterial culture is to lessen the chances of bacterial variability within this experiment. It has been shown that although PAO1 is the most commonly used strain of *P. aeruginosa* for laboratory tests, there have been reports of genomic variability within this strain (Klockgether *et al.*, 2010).

3.2 Experimental Methods

3.2.1 Size Analysis

The size of the nanoparticles was assessed by dynamic light scattering (DLS) using a Brookhaven ZetaPALS machine, for IS of 1 and 25 mM NaCl, and a pH of 7.5 ± 0.1 (controlled by addition of small amounts of 0.01M NaOH or HCl). These measurements were done 10 times, with a scattering angle of 90°, a wavelength of 660 nm and a controlled temperature of 24 ± 1°C. The

DLS results were then qualitatively compared to images from a JAMP-9500F (JEOL) SEM run at 25.0 keV, and a JEM2100 (JEOL) transmission electron microscope (TEM) run at 120 keV.

Dynamic Light Scattering

DLS, also referred to as photo correlation spectroscopy, or quasi-elastic light scattering, indirectly determines the size of particles through measurement of the interference patterns of a light source. Particles move due to thermal fluctuations (Brownian motion), and smaller particles move faster than their larger counterparts. Thus, through measuring the rate of decay of the changes in light intensity, the diffusion constant (D) can be determined. Finally, through use of the Stokes-Einstein relationship [Equation (3.1)], the hydrodynamic radius (R_h) of the particles can be determined using the Boltzmann constant (k_B), temperature (T) and the liquid viscosity (μ) as the input parameters.

The assumption used for the size determination is that the particle is spherical, so that the radius (R) equals to R_h. It has been shown that this technique can give accurate size determinations for monodisperse particles within a few percent, and that the sizes of moderately polydisperse particles can also be determined (Holmberg, 2002).

$$D = \frac{k_B T}{6\pi\mu R_h} \tag{3.1}$$

3.2.2 Zeta Potential Determination

The electrophoretic mobilities of nanoparticles, bacterial cells and crushed glass beads, for IS of both 1 and 25 mM NaCl, at a pH of 7.5 ± 0.1, were measured using a Brookhaven ZetaPALS machine. The measurements were averaged over at least 5 runs of 20 cycles, at a temperature of 24 ± 1°C. The mobilities were then converted to zeta potentials using the Smoluchowsky equation (see Equation (3.2).

Zeta potentials of the bacteria, at 1 and 25 mmol, were determined by preparing a cellular suspension, as described above, then washing three times. The washing procedure involved pipetting a 2 mL sample of the suspension into a 2 mL micro-centrifuge tube, and centrifuging in an Eppendorf 5415R at 4000 RPM for 5 minutes. The supernatant was then removed, and 1 mL of a 0.9% (w/v) NaCl buffer solution was added, vortexed to mix the pellet of cells, centrifuged again, then repeated. After discarding the supernatant the last time, the 1 or 25 mmol solution, at a pH of 7.5 was added, and then vortexed. 40 μL of the resulting suspension was then added to 2 mL of the proper molar solution, and measured for zeta potential as described above.

Phase Analysis Light Scattering

The technique used by, and namesake of the ZetaPALS machine, is phase analysis light scattering (PALS). This technique determines the electrophoretic mobilities of particles by modulating the phases of a reference light beam and electric field. The scattered light beam is Doppler shifted due to the movement of the particle in the electric field. By constructing a plot of the

phase shift of the reference and scattered light beams over a number of cycles, the velocity of the particles can be determined (Cosgrove, 2005). In order to convert electrophoretic mobility to zeta potential, the forces that govern the motion of the particle must be accounted for. Using the Smoluchowski equation (Equation (3.2); valid for most particles in aqueous media), the zeta potential (ϕ) is related to the velocity of the particle (v_p), the viscosity of the media (μ), the electric field (E) and the permittivity of the solvent ($\epsilon\epsilon_0$) (Cosgrove, 2005).

$$\phi = \frac{v_p \mu}{E \epsilon \epsilon_0} \tag{3.2}$$

3.2.3 Electron Microscope Imaging

Images used for qualitative comparisons like nanoparticle size and biofilm coverage on porous media were taken with a SEM or a TEM. The background theoretical information, as well as sample preparation for each of these methods will be discussed.

Scanning Electron Microscope

A SEM has a lower resolution than a TEM, but requires less invasive processing of the sample. Although there are several common modes of operation for a SEM, including the detection of backscatter electrons, characteristic X-rays and secondary electrons, in this study we solely made use of the latter.

Topographic images are collected from low energy secondary electrons that are ejected from the sample due to collisions with high energy electrons origi-

nating from a tungsten electron gun that raster scans the sample. The image is constructed by the varying intensities of electrons that hit the detector due to variations in the angle of incidence of the incoming electron beam and the sample, and the position of the detector.

In order to make use of the SEM, a sample must be both dry and conductive. Due to the presence of a very high vacuum, hydrated (biological) samples are impossible to image without breaking apart, and are thus chemically preserved, or 'fixed'. The high vacuum is needed for the SEM (as well as the other techniques described) in order to ensure both a contamination free environment, and reduce collisions of the electron beam with gas or other molecules. A sample's conductivity, if needed, can be improved through coating in electrically conductive materials.

In this experiment, the iron nanoparticles were simply dried onto a sample holder and imaged in a JEOL JAMP-9500F. However, the glass beads containing the biofilm were heavily processed via the following protocol:

1. Upon sample retrieval, immediately place into 2.5% glutaraldehyde in Millonig's buffer and store at 4°C
2. Wash in the same buffer 3 times for 10 minutes each
3. Postfix in 1% OsO_4 at room temperature for 1 hour
4. Briefly wash in distilled water
5. Serial dehydration in ethanol (50%–100%) for 10 minutes each, followed by 2 additional applications of absolute ethanol for 10 minutes each.

6. Critical point dry at 31°C for 5–10 minutes

7. Mount on stub with silicon membrane

8. Sputter coat with gold in an Edwards S150B Sputter Coater

9. Image in a Hitachi SEM S-2500

Transmission Electron Microscope

A TEM allows for high resolution images to be taken at larger magnifications than attainable for a SEM. The main operational difference between a SEM and a TEM is that electrons pass through the sample and are collected. Therefore, bright areas on images are void of atoms, while dark spots indicate their presence. Only iron nanoparticles were imaged by TEM, and the preparation was minimal, with an air dried sample scattered onto a formvar coated grid and imaged in a JEOL TEM JEM2100.

3.2.4 Compositional Analysis

The surface composition of the pnZVI was determined from both Auger electron spectroscopy (AES) and X-ray photoelectron spectroscopy (XPS). The principles behind these spectroscopic methods will be discussed.

Auger Electron Spectroscopy

AES can be used to detect the chemical composition of the top 3 to 5 nm of a sample, with a spatial resolution of approximately 250 nm. The only elemental limitations of AES are hydrogen and helium, due to the absence of

valence band electrons. With a setup similar to that of a SEM, an electron source bombards a sample, in a high vacuum, with high energy electrons. However, unlike a SEM, AES does not measure the secondary electrons that are released from the sample via collisions with the primary beam. Once a core electron is removed, an outer shell electron replaces it and due to the lower energy associated with the ground level, the replacement electron gives off some energy. This energy can then be absorbed by an outer shell electron. If the absorbed energy is sufficient to overcome the electron's binding energy, it is emitted. The energy of this emitted outer shell electron is then measured by the Auger detector.

Due to the very specific orbital energy levels of different elements, the measured kinetic energy of the emitted electron can be used to back calculate the element that it came from. This is done by using Equation (3.3), with E_k representing the kinetic energy of the emitted outer shell electron, E_{core} equal to the binding energy of the removed core electron and E_B and E_C representing the binding energies of the electron that replaced the core electron and the subsequently ejected electron, respectively. Due to the presence of multiple outer shells, there can be many peaks associated with each element. However, AES has matured as an analytical tool, therefore many databases exist containing expected Auger electron energies for all of the elements.

Samples of iron nanoparticles were simply air dried onto the sample holders and analyzed by AES in a JEOL JAMP-9500F.

$$E_k = E_{core} - E_B - E_C \tag{3.3}$$

X-ray Photoelectron Spectroscopy

XPS can be used to ascertain compositional data from the top couple of nm of a sample by exploiting a different mechanism to the one used by AES. Elemental limitations of XPS are again hydrogen and helium, but this time the limitation is due to the small orbital diameter reducing the interaction of the incident photon and electron to near zero. In XPS, a sample, under high vacuum, is bombarded with lower energy X-rays from an Aluminum (1486.6 eV) source, rather than electrons, leading to a reduced spatial resolution, but imparting less damage to the sample. The X-rays excite the inner shell electron of an atom, causing their ejection due to the photoelectric effect (Einstein, 1905). Each electron has a kinetic energy characteristic of the material it originated from, with distinctions between different chemical states possible. In Chapter 4, the notation C 1s, Fe 2p etc. will be used to describe the data. C and Fe are the elements, in this case carbon and iron, while 1s and 2p are the atomic notation used to describe the quantum numbers associated with the orbit (n, described by an integer number) and orbital angular momentum (l, described by the letters s, p, d and f denoting the l numbers 1 to 4). There are also quantum numbers for spin angular momentum (s) and total angular momentum (j) that will not be presented in this current research. However, due to these quantum considerations, the binding energies of s orbitals show up in XPS data as one peak, while the p, d and f orbitals exhibit split peaks, due to spin orbital splitting.

Data from an XPS analysis is output in the form of counts of electrons

versus the binding energy. The position of the peaks indicate the elemental composition of the source, while the shape of the curve is indicative of the different chemical states of the element. The local chemical or physical environment and oxidation state will affect the binding energy of a material. Therefore, by analyzing the placement and shapes of the resulting peaks, and comparing to other XPS results for known compounds, this information can be gathered. Equation (3.4) shows how the binding energy (E_b) can be found from experimentally measurable values of the incident X-ray energy (E_p, p for photon), the kinetic energy of the measured electron (E_k), and the instrument detector dependent value of the work function (δ).

$$E_b = E_p - E_k - \delta \tag{3.4}$$

3.2.5 Preparation of Experimental Columns

Uncoated Columns

Prior to each use, the glass beads were thoroughly cleaned with both acid and base via the following protocol (Li *et al.*, 2006):

1. Wash with ultra pure water
2. Ultrasonicate in 0.01 M NaOH for 15 min
3. Ultrasonicate in ultra pure water and repeat until rinsed solution becomes transparent
4. Ultrasonicate in 1 M HNO_3 for 20 min

5. Final rinse with ultra pure water

The wet packed cast acrylic experimental columns used were 14 cm long, with an inner diameter of 3.175 cm ($1^{1/4}$ in.), and a porosity of 0.40. At each end, a 40 mesh stainless steel screen was used to support the filter media, as well as to disperse the influent.

Biofilm Coated Columns

The coated columns were initially prepared using the same protocol as the uncoated ones. The procedure used for coating biofilm in the packed columns is similar to the one described in previous studies (Liu and Li, 2008; Tong *et al.*, 2010).

To grow the biofilm, a cellular suspension was prepared, as outlined above. The column was seeded with bacteria by recirculating the cellular suspension, in the upflow direction, for 12 hours using a MasterFlex L/S peristaltic pump, with size 13 peroxide cured silicon tubing (Cole Parmer), at a flowrate of 1.05 $\pm$ 0.02 mL/min. After seeding, the biofilm was grown by injecting a 1/5th dilution of LB broth at a flowrate of 1.05 $\pm$ 0.02 mL/min for 5 days, switching the direction between upflow and downflow every 12 hours to allow for uniform formation of the biofilm.

The distribution of biofilm bacteria number was determined by growing two columns, extracting the porous media into five separate segments into a solution of phosphate buffered saline, then sonicating the media for 10 minutes, before preforming duplicate plate counting with the resulting suspension using the drop plate method (Liu and Li, 2008). Ten minutes of sonication was shown

to produce less than 0.1% cell lysis in a previous study using *P. aeruginosa* bacteria (Liu and Li, 2008).

3.2.6 Iron Transport Experiment

Prior to iron injections, the columns were pre-conditioned with at least five PVs of either 1 or 25 mmol NaCl, with a pH of 7.5 ± 0.1 at an environmentally relevant flowrate equivalent to 8.3 ± 0.2 m/d, introduced in the upflow direction. This flowrate was chosen specifically because it is in the range of groundwater flowrates, and to compare the present results to those of Tong *et al.* (2010), who used a flowrate of 8 m/d. During the conditioning period, an aliquot of NANOFER 25S was drawn from the supernatant of the solution stored in the fridge. This aliquot was then added to a prepared solution of either 1 or 25 mmol NaCl and adjusted to a pH of 7.5 ± 0.1. The resulting concentrations were between 106 and 171 mg/L of total iron for all trials. The equivalent of two PVs of the iron solution was then injected into the column in the upflow direction at 8.3 ± 0.2 m/d, followed by three PVs of either 1 or 25 mmol NaCl solution. Elutions were collected in half PV aliquots, and analyzed for total iron by the phenanthroline complexation method (AWWA, 1992), as described below.

Iron Determination

3 mL of sample was added to ∼50 mL of ultra pure water to dilute the sample, along with 2 mL of HCl to lower the pH, and 1 mL of hydroxylamine hydrochloride and brought to a boil with two glass beads, to ensure all iron

is reduced to its ferrous form. The solution was then boiled down to 15 to 20 mL and allowed to cool. 10 mL of ammonium acetate buffer was then added, followed by 4 mL of 1,10 phenanthroline monohydrate to chelate with the ferrous iron. The chelation creates an orange-red color that was measured at 510 nm and compared to a standard curve made from known quantities of ferrous ammonium sulphate iron standard.

3.2.7 Model Development

T-E Model

The T-E model [Equation (2.7)] was used to calculate the theoretical η_0 for the column experiments, with and without the presence of biofilm. The relationships used to calculate η_0 are given in Equations (3.5) to (3.10), and described below, with the values used listed in Table 3.1.

$$A_S = \frac{2(1-\gamma^5)}{2-3\gamma+3\gamma^5-2\gamma^6}, \qquad \gamma = (1-f)^{1/3} \tag{3.5}$$

$$N_R = d_p/d_c \tag{3.6}$$

$$N_{Pe} = \frac{Ud_c}{D_\infty}, \qquad D_\infty = \frac{k_B T}{3\pi\mu d_c} \tag{3.7}$$

$$N_{vdW} = \frac{A_{123}}{k_B T}, \qquad A_{123} = (\sqrt{A_{11}} - \sqrt{A_{33}})(\sqrt{A_{22}} - \sqrt{A_{33}}) \tag{3.8}$$

$$N_A = \frac{A_{123}}{3\pi\mu d_p^2 U} \tag{3.9}$$

$$N_G = \frac{1}{9}\frac{d_p^2(\rho_p - \rho_f)g}{2\mu U} \tag{3.10}$$

A_S [Equation (3.5)] is a function dependent on the porosity of the porous media, with the variable γ defined as a direct function of the porosity (f). N_R [Equation (3.6)] is the aspect ratio, or ratio of the particle (d_p) and collector (d_c) diameters. N_{Pe} [Equation (3.7)] is the Peclet number that describes the ratio of convective transport to diffusive transport, with U and and D_∞ representing the approach velocity of the fluid and the diffusion coefficient, respectively. D_∞ is further defined by parameters of Boltzmann constant (k_B), absolute temperature (T) and the absolute fluid viscosity (μ). N_{vdw} [Equation (3.8)] is the van der Waals number, which is the ratio of the particle's van der Waals interaction (via the system Hamaker constant, A_{123}) to its kinetic energy. The system Hamaker constants (A_{123}) were estimated using the equation from Israelachvili (1992), as shown in Equation (3.8), with A_{11}, A_{22} and A_{33} being the Hamaker constants of the colloid, collector and water, respectively. N_A [Equation (3.9)] is the attraction number, which is a combination of the van der Waals and fluid velocity forces as they relate to interception. Lastly, N_G [Equation (3.10)] is the gravity number, which is the ratio of the Stokes particle settling velocity and the fluid approach velocity, with ρ_p, ρ_f and g representing the particle density, the fluid density and the acceleration due to gravity. All of the input parameters, with the exception of the Hamaker

Table 3.1: Parameters used for the T-E model.

Symbol	Value Used
f, porosity	0.40
d_p, particle diameter (m)	60E-9
d_c, collector diameter (m)	0.55E-3
U, fluid approach velocity (m/s)	97.2E-6
T, temperature (K)	293
μ, fluid viscosity of medium (Pa s)	1.005E-3
A_{11}, Hamaker constant of pnZVI (J)	10E-20
A_{22}, Hamaker constant of glass beads (J)	12.1E-20
A_{22}, Hamaker constant of bacteria (J)	4.8E-20
A_{33}, Hamaker constant of water (J)	3.7E-20
A_{123}, Hamaker constant (biofilm) (J)	0.33E-20
A_{123}, Hamaker constant (no biofilm) (J)	1.9E-20
ρ_p, particle density (kg/m^3)	5700
ρ_f, fluid density (kg/m^3)	1000

constants, were either readily measured or theoretical constants.

The Hamaker constant of 10E-20, used for pnZVI, was used previously in two different studies with nZVI coated with guar gum and CMC (Tiraferri and Sethi, 2009; Fatisson *et al.*, 2010). The Hamaker constant used for the glass beads (12.1E-20) was reported by Takase (2009), while the Hamaker constants commonly used for bacteria (4.8E-20) and water (3.7E-20), were reported by Triandafillu *et al.* (2003) and Israelachvili (1992), respectively. The resulting system Hamaker constants were within the range of those used by Tufenkji and Elimelech (2004a).

DLVO Model

The DLVO model was used to investigate the removal of pnZVI based on the summation [Φ_{total}(h)] of electrostatic [Φ_{el}(h)] and retarded van der Walls [Φ_{vdW}(h)] interaction energies [Equation (3.11)] (Derjaguin and Landau, 1941;

Verwey, 1947) as a function of the distance between two spheres. The relations used in the calculation of the electrostatic and retarded van der Waals forces for a sphere-sphere interaction are shown in Equations (3.12) and (3.13) (Bradford and Torkzaban, 2008) and Equation (3.14) (Gregory, 1981). Relevant parameters defined and presented for the T-E Model in Table 3.1 are reused, while new parameters relevant for the DLVO model are introduced below, with their values listed in Table 3.2.

The electrostatic interaction energy between two spheres, Φ_{el}(h) [Equation (3.12)] is governed by parameters of permittivity ($\epsilon\epsilon_0$), particle and collector radii (r_p and r_c), particle and collector surface potentials, with zeta potentials used in their stead (ϕ_p and ϕ_c), inverse of the double layer thickness [κ, with new parameters of electron charge (e), Avogadro's number (N_{Av}), molar concentration of the electrolyte (M_i) and the valence of the electrolyte (z)] and the distance between the two spheres (h). The retarded van der Walls interaction between two spheres, Φ_{vdW}(h) [Equation (3.14)] uses only one previously undefined parameter, the characteristic wavelength (λ_c) (Gregory, 1981).

Due to the small size of the modeled particle, the sphere sphere interaction could have been simplified to a sphere plane interaction, with $r_p r_c/(r_p+r_c)$ being replaced with r_c in Equations (3.12) and (3.14), however, the results would remain identical. All of the values used for this model were either fundamental constants, or experimentally measured.

$$\Phi_{total}(h) = \Phi_{el}(h) + \Phi_{vdW}(h) \tag{3.11}$$

Table 3.2: New parameters introduced for the DLVO model.

Symbol	Value Used
r_p, particle radius (m)	30E-9
r_c, collector radius (m)	0.275E-3
ϵ, relative permittivity	80.36
ϵ_0, permittivity in a vacuum (F/m)	8.85E-12
ϕ_p, zeta potential of particle (1 mmol) (mV)	-36.25
ϕ_p, zeta potential of particle (25 mmol) (mV)	-16.75
ϕ_c, zeta potential of uncoated collector (1mmol) (mV)	-67.03
ϕ_c, zeta potential of uncoated collector (25mmol) (mV)	-50.73
ϕ_c, zeta potential of coated collector (1mmol) (mV)	-41.70
ϕ_c, zeta potential of coated collector (25mmol) (mV)	-25.96
N_{Av}, Avogadro's number (molecules/mole)	6.02E23
M_i, molar concentration of electrolyte (mmol/L)	1 or 25
e, electron charge (C)	1.602E-19
z, electrolyte valence	1
λ_c, characteristic wavelength (m)	1E-7

$$\Phi_{el}(h) = \frac{\pi\epsilon\epsilon_0 r_p r_c}{(r_p + r_c)} \left(2\phi_p\phi_c ln\left(\frac{1 + exp(-\kappa h)}{1 - exp(-\kappa h)}\right) + (\phi_p^2 + \phi_c^2) ln\left(1 - exp\left(-2\kappa h\right)\right)\right) \tag{3.12}$$

$$\kappa = \sqrt{\frac{2000 e^2 N_{Av}}{\epsilon k_B T} \sum_i M_i z_i^2} \tag{3.13}$$

$$\Phi_{vdW}(h) = -\frac{A_{123} r_p r_c}{6h(r_p + r_c)} \left(1 - \frac{5.32h}{\lambda_c} ln\left(1 + \frac{\lambda_c}{5.32h}\right)\right) \tag{3.14}$$

Chapter 4

Results

4.1 Nanoparticle Characterization

4.1.1 Size

The average diameter of the iron nanoparticles, as determined by the DLS measurements, were 61 ±2 nm (polydispersity of 0.15 ±0.03), and 59 ±3 nm (polydispersity of 0.18 ±0.03), for the 1, and 25 mmol NaCl IS, respectively. Figure 4.1 a and b, an SEM and TEM image from a JEOL JAMP-9500F and JEOL JEM2100, respectively, show dried samples of iron nanoparticles, drawn from the supernatant of the stored iron particles from the fridge. This image shows the size of the nanoparticles to be in qualitative agreement with the DLS results of ∼60 nm. Klimkova *et al.* (2011) also found that the average size of NANOFER 25S was 60 nm, determined from TEM measurements.

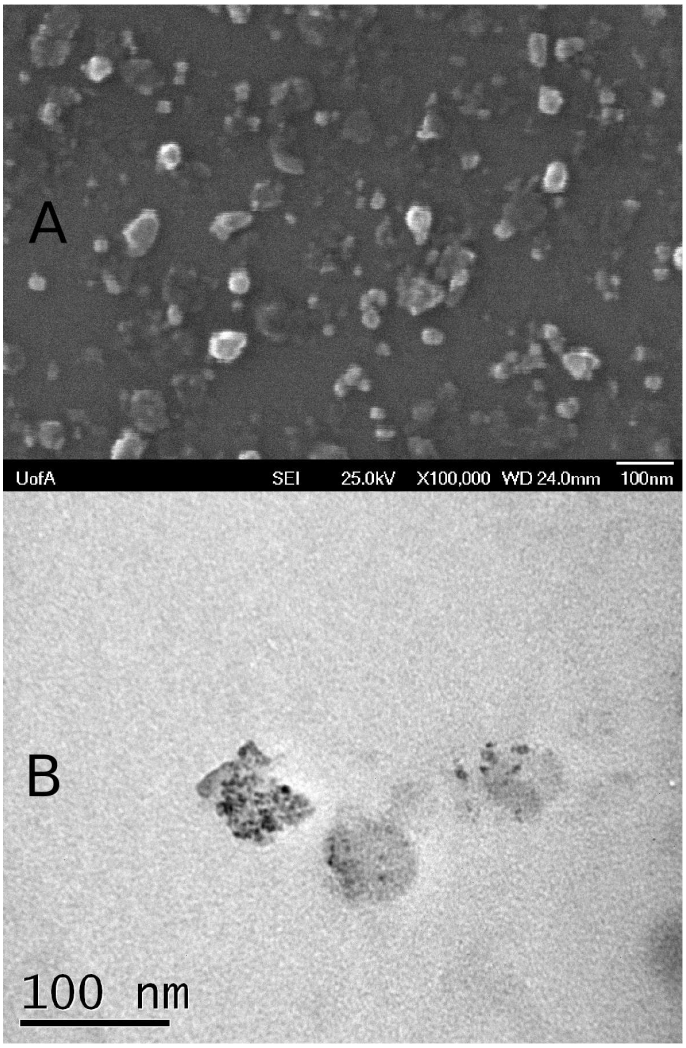

Figure 4.1: A) SEM image (JEOL JAMP-9500F) and b) TEM image (JEOL JEM2100) of a dried sample of pnZVI drawn from the supernatant of stored particles. An average size of ∼60 nm was measured with DLS, and is qualitatively confirmed in these images.

4.1.2 Zeta Potential

The zeta potentials of the pnZVI were determined to be -36.25 ±3.28 in the 1 mmol NaCl solution, and -16.75 ±2.00 for the 25 mmol IS. The measurement of the absolute magnitude of the zeta potential decreased with increasing electrolyte concentration due to EDL compression at the higher IS.

4.1.3 Surface Composition

Auger Electron Spectroscopy

The surface composition of the pnZVI was determined from AES spectra. Two typical spectral plots are shown in Figure 4.2. The top (solid) line is the AES spectra collected from a particle of pnZVI (seen as a white spot in Figure 4.1a) while the bottom (dashed) line is a spectrum collected from an area of the sample void of any pnZVI. The text labels identify the peaks of the elements observed in the Auger spectra: carbon at 272 eV, oxygen at 484 and 505 eV, iron at 598, 651 and 703 eV, sodium at 990 eV and silicon at 1561, 1583, 1601 and 1619 eV. The Auger peaks for carbon, oxygen, silicon, and to a very small degree, sodium, are present in both scans. However, the three peaks indicative of iron, as well as a larger relative intensity for sodium, are only present in the scan of an identifiable nanoparticle. Carbon and oxygen are abundant in the environment, thus show up regularly in AES scans, while silicon is present due to its use as the sample holder. The large intensities for iron and sodium in the composition of the pnZVI are expected, as the surface coating of the iron, as indicated by the company Nano Iron S.R.O. (private communication),

is due to preparation in 3% sodium poly(acrylic acid) (Na-PAA).

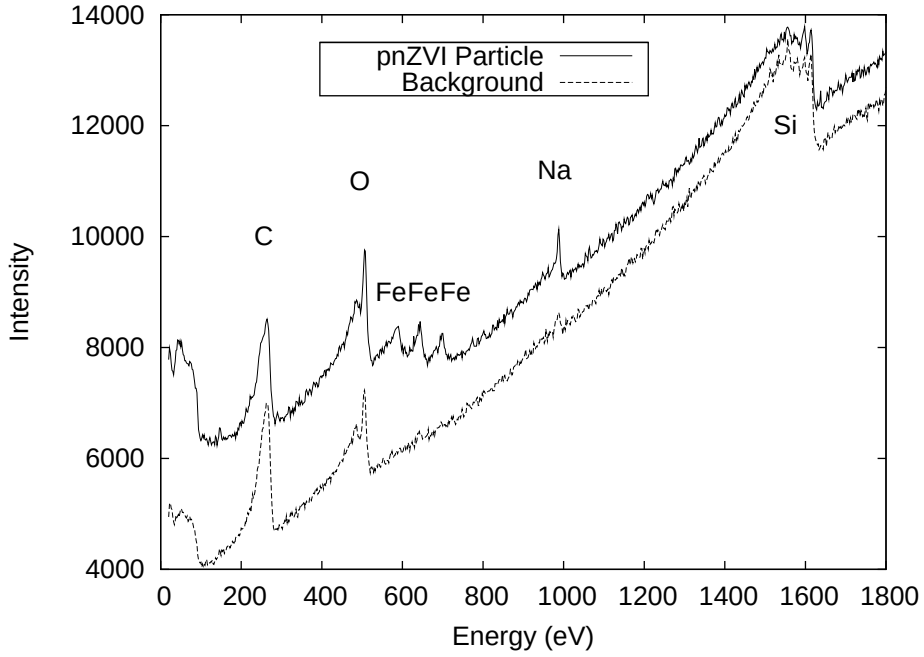

Figure 4.2: Energy spectra of Auger electrons collected from a portion of sample containing pnZVI (solid line), and void of pnZVI (dashed line), shown in Figure 4.1a. Text labels identify the elements corresponding to the energy peaks. The pnZVI spectrum shows the presence of iron as well as significantly more sodium than background, due to the use of Na-PAA during the manufacturing of pnZVI.

X-ray Photoelectron Spectroscopy

An XPS analysis of the sample surface was also employed in order to quantify the composition of the pnZVI. In survey mode, shown in Figure 4.3 with labels for the prominent peaks, data indicated a chemical makeup similar to that reported from AES, including strong intensities for binding energies typical of carbon (C 1s, 286.2 eV), oxygen (O 1s, 532.2 eV), sodium (Na 1s, 1072.2 eV) and iron (Fe 2p, 712.6 eV). Noteworthy is the presence of the doublet peak, expected for Fe 2p, due to the spin orbital splitting of the p subshell. The other

labels, O Auger and Na Auger, show the observation of Auger peaks in the data that are common in XPS scans. The calculated composition, averaged over a dried sample of about 300 x 700 μm, was 45% carbon, 33% oxygen, 16% sodium and 4% iron, by mass. Additionally, in order to confirm the presence of Na-PAA, high resolution spectra for carbon (C 1s, Figure 4.4a) and oxygen (O 1s, Figure 4.4b) were collected.

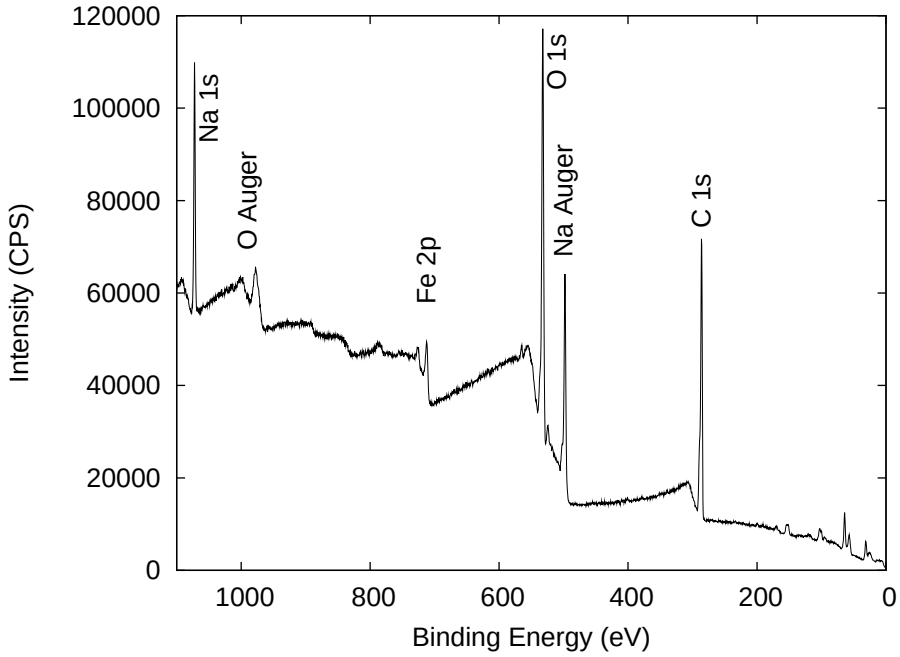

Figure 4.3: XPS data from a survey mode scan of pnZVI. Text labels indicate the elements corresponding to the large peaks in the graph.

The C 1s carbon data were successfully fit by using component analysis (CASA XPS software), similar to Alexander *et al.* (2001), with five Gaussians corresponding to expected carbon bonds [see Table 4.1 for the components, peaks positions and full width at half maximum (FWHM)] present in a thick film of Na-PAA. This figure shows that the summation (solid line) of the Gaussian components (dashed lines), closely matches the collected XPS data (dots).

The molecular weight of the Na-PAA used in the manufacturing of NANOFER 25s is not known. However, due to the lower composition percentage of the C-OX (X=H, or Na) component at 287.1 eV that is associated with end groups [2 % in this study versus 4 % in Alexander *et al.* (2001)], NANOFER 25S likely uses Na-PAA with a molecular weight greater than the 6000 g/mole sample used by Alexander *et al.* (2001). The peaks of these curves are offset towards higher bonding energies than those presented by Alexander *et al.* (2001) for pure Na-PAA, but are similar to range of C 1s data measured for PAA bonded to oxidized metals (Leadley and Watts, 1997) and pseudoboehmite (Alexander *et al.*, 2001). The increased binding energy measured is therefore likely due to oxidation, or the presence of the iron in this sample that would change the electrostatic shielding due to the withdrawal of valence electrons.

High resolution oxygen (O 1s) data was also fit similarly to the O 1s spectra for Na-PAA presented in Alexander *et al.* (2001) (see Table 4.1), with one additional component needed to represent an O-Fe bond, at 530.0 eV, due to the oxidized iron shell of pnZVI. As with the carbon peaks, the binding energies are shifted to higher values than those reported in Alexander *et al.* (2001) for pure Na-PAA, again likely due oxidation, or the attachment to iron.

4.2 Porous Media Characterization

4.2.1 Zeta Potential

The zeta potentials of crushed soda-lime glass beads for 1 and 25 mmol NaCl were determined to be -67.03 ±2.49 mV and -50.73 ±0.51 mV, respectively.

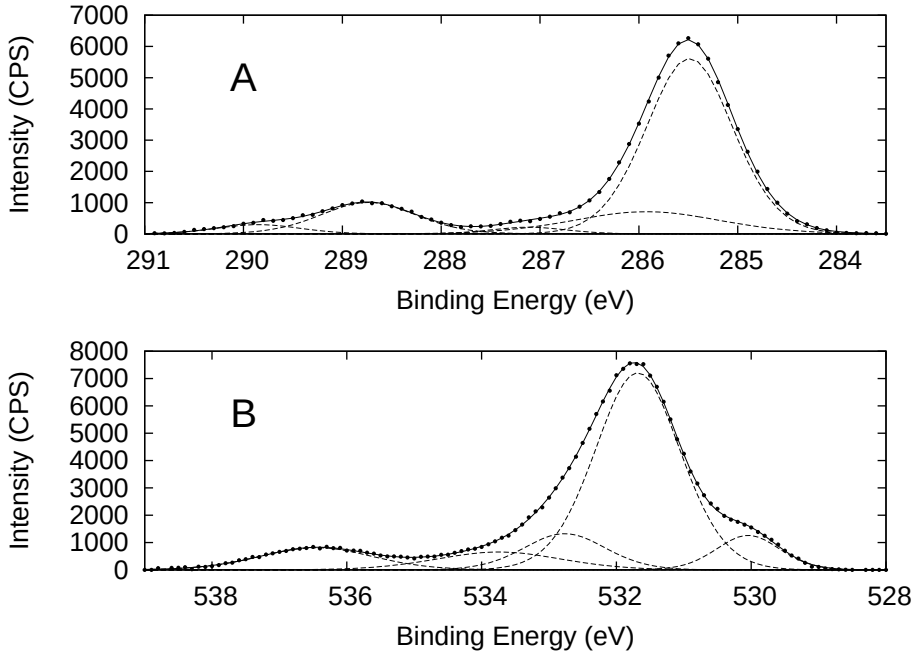

Figure 4.4: High resolution energy spectra of a) C 1s and b) O 1s binding energies calculated from XPS data. The dashed lines are Gaussians used to model expected bonds in Na-PAA. The summation of the Gaussian components (solid line) matches the XPS data (dots) very closely.

Table 4.1: Components, peak positions and FWHM for Gaussian fitted spectra illustrated in Figure 4.4.

Bond Type	Binding Energy (eV)	FWHM (eV)
Figure 4.4a C 1s		
C-C/CH	285.5	1.03
$\underline{C}$-CO_2X, X=H or Na	285.9	1.76
$\underline{C}$-OX	287.1	0.89
C-$(O\text{-}Na)_2$	288.7	1.13
C(=O)OH	289.8	0.98
Figure 4.4b O 1s		
Fe-O	530.0	1.10
-O-Na	531.7	1.49
C(=$\underline{O}$)OH	532.8	1.42
C(=O)$\underline{O}$H	533.7	2.19
Na KVV	536.5	1.97

Washed cells of *P. aeruginosa* bacteria exhibited zeta potentials of -41.70 ±1.50 mV for 1 mmol NaCl, and -25.96 ±2.20 mV for 25 mmol NaCl. These results are consistent with compression of the EDL leading to lower zeta potentials at higher IS.

4.2.2 Bacterial Dispersion

Viable bacterial counts of *P. aeruginosa* through the columns are presented in Figure 4.5. This figure shows that the dispersion of the bacteria is nearly homogeneous when considering the error bars (standard deviations of 4 data points), with quantities of cells $\sim 10^7$ CFU/gdw, within the range of reported values of viable bacteria cells found in saturated aquifers (Balkwill and Ghiorse, 1985; Bone and Balkwill, 1988; Wilson *et al.*, 1983; Webster *et al.*, 1985). The distribution of EPS through the columns was not measured for this study. However, using a similar growth protocol, Liu and Li (2008) attained similarly homogeneous bacterial counts, and showed that the concentration of EPS was also homogeneous throughout their experimental column.

4.2.3 EPS Components

The major component of *P. aeruginosa* PAO1 biofilm is known to be carbohydrates (Liu and Li, 2008). The majority of the carbohydrates for a *P. aeruginosa* (PAO1) biofilm, grown with LB broth on the insides of silicone tubing, were shown to be glucose, rhamnose, and mannose (Wozniak *et al.*, 2003). These neutral sugars partially block the negatively charged functional

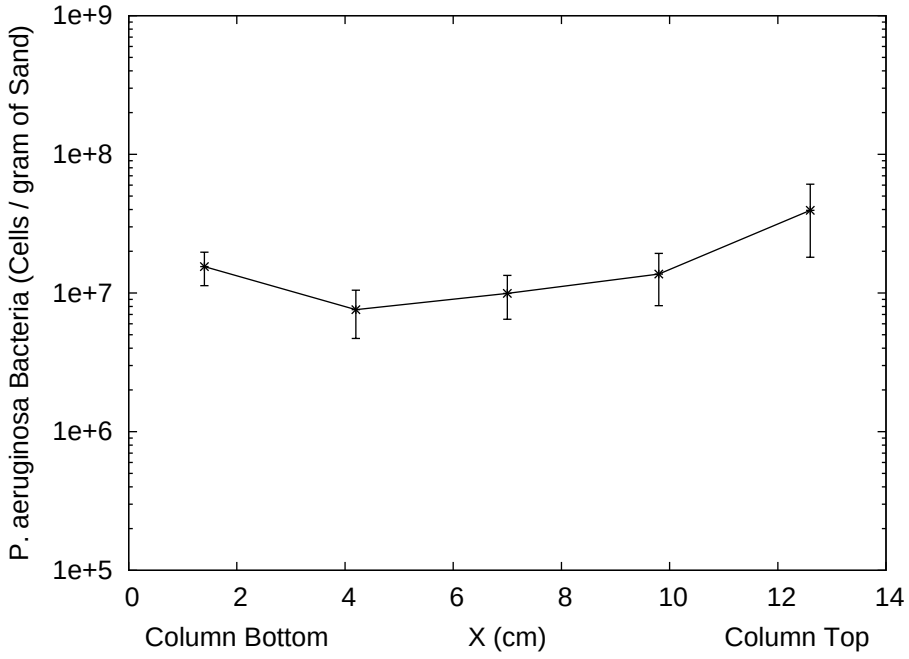

Figure 4.5: Number of *P. aeruginosa* bacterial cells per gram of dry sand throughout the columns. Error bars represent standard deviations of duplicate measurements of two separate columns (four data points).

groups that are found on the cellular surface, leading to a neutrally charged biofilm (Liu *et al.*, 2007).

4.3 Iron Transport

4.3.1 Iron Elution

Results of the iron elution studies are shown in Figure 4.6 a and b, showing the normalized effluent iron concentrations (C/C_0), for the 1 and 25 mmol NaCl concentrations, respectively, of biofilm coated and uncoated columns. The error bars signify standard deviations of duplicate phenanthroline iron analysis of duplicate columns (4 data points). As samples were collected in

half PV aliquots, with injections beginning at PV equal to zero, the skewed measurements at 1.0 (higher than expected) and 3.0 PV (lower than expected) indicate the likelihood of preferential flow paths through all of the columns. There is also no noticeable tail for any of the breakthrough curves, suggesting that all filtered pnZVI were retained in the column. The measurements at 1.5 to 2.5 PVs form a constant plateau (within error) suggesting that a steady state of particle removal was achieved.

The main result of these breakthrough experiments is that only the biofilm covered column at the higher IS shows significant filtration of pnZVI. To better quantify the transport, an effective plateau value of breakthrough curves (Lecoanet and Wiesner, 2004) was calculated using an average of the C/C_0 values from the elutions at 1.5, 2.0 and 2.5 PVs. For the 1 mmol solution IS, the iron breakthrough plateau for the biofilm coated and uncoated porous media were measured to be 97 ± 6% and 96 ± 4%, respectively. The columns with increased IS resulted in iron breakthroughs of 82 ± 3% and 97 ± 2% for the coated and uncoated columns.

4.3.2 Iron Recovery

Total iron recovery for both columns at the 1 mmol IS, as well as the uncoated column at the high IS were all within error of 100%, while the recovered iron from the biofilm coated column at 25 mmol IS was 79 ± 6%. These recoveries are reasonable when compared to Tong *et al.* (2010), who also showed a marked increase of nanoparticle retention in biofilm coated columns, only at higher IS. Additionally, it has been shown by column breakthrough studies that snZVI

is not retained in porous media at IS less than 40 or 100 mmol of Na^+ (Saleh *et al.*, 2008), and IS less than 40 mmol of Ca^+ (Lin *et al.*, 2010), depending on the applied coating. As it has been suggested that PAA is one of the best modifications with respect to nZVI transport (Yang *et al.*, 2007), the high value of 25 mmol IS is likely not large enough to impact the transport of pnZVI in the uncoated columns used in this study. These results will be further discussed in the context of the T-E model and DLVO theory in the following sections.

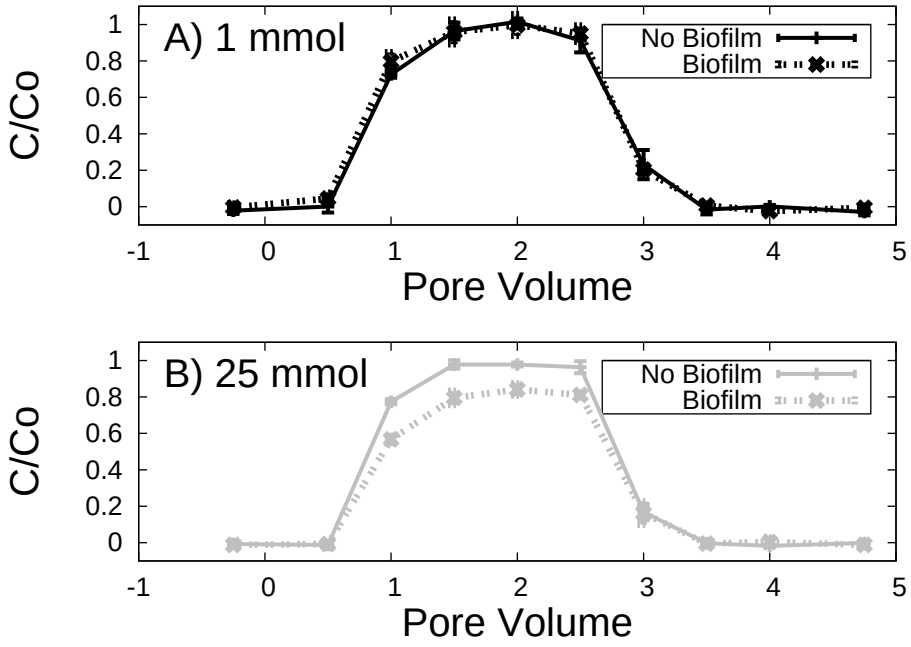

Figure 4.6: Iron breakthrough curve for uncoated and *P. aeruginosa* biofilm coated porous media for the a) 1 mmol and b) 25 mmol NaCl ISs. Error bars indicate standard deviations of duplicate iron measurements from two separate columns (4 data points).

4.4 T-E Model

The results of the T-E model indicate that for pnZVI in the experimental conditions, η_0 is expected to be 3.11E-2 for biofilm coated porous media, and 2.84E-2 for uncoated porous media. The only factor that differs for the biofilm coated and uncoated experimental setups that is taken into account by the T-E model is the different Hamaker constants. Specifically, the T-E model does not take into account the DLVO forces that are affected by changes in surface charge of the particles and collectors with changing solution IS (Tufenkji and Elimelech, 2004b). Thus, the relative values of η_0 should only be useful in predicting differences between biofilm coated and uncoated columns at the same solution IS. Values of η and α were calculated from Equations (2.7) and (2.8) and the experimental iron breakthroughs, and are presented in Table 4.2. The highlight of the T-E results is the larger relative value of attachment efficiency (α) and therefore single collector removal efficiency (η) for the biofilm coated experiment at 25 mmol IS, as compared to the uncoated media. The lower Hamaker constant input to the T-E model for the bacteria coated beads serves to lower the expected η_0 value, as compared to uncoated beads, thus decreasing the expected particle removal for a given set of physiochemical conditions. The difference in α must therefore be due to other forces allowing for more favorable attachment in the biofilm coated porous media.

These results must be interpreted cautiously however, as the input parameter of the collector Hamaker constants for the biofilm coated media were chosen for the ideal condition of complete coverage of the glass beads by bac-

Table 4.2: T-E model outputs.

Parameter	Biofilm (1mM)	No Biofilm (1mM)	Biofilm (25mM)	No Biofilm (25mM)
η_0x10^{-2}	2.84	3.11	2.84	3.11
C/C_0	0.97	0.96	0.82	0.97
αx10^{-3}	4.69	5.72	30.5	4.27
ηx10^{-4}	1.33	1.78	8.66	1.33

terial cells. This ideal situation is not occurring due to incomplete coverage of all beads by biofilm, verified by SEM images and shown below in Figure 5.1. In addition, the Hamaker constant of the biofilm is assumed to be the same as that used for bacterial cells. However, because the Hamaker constant is proportional to the density of the material, soft EPS would have a Hamaker constant more similar to the soft bacterial cells than to the hard glass beads. Even with these caveats, a different Hamaker constant for the biofilm covered porous media would not substantially change the interpretation of the results of the model due to the significantly larger value of α for the biofilm coated column at the higher IS.

4.5 DLVO Model

The DLVO model will serve to elucidate whether the increased α, as measured by the particle breakthrough curves, is due to electrostatic and van der Waals forces.

Through use of different scales for the interaction energy, Figure 4.7 a and b show the repulsive energy barriers and the secondary minimums of the particle-collector interactions in this study, respectively, in units of k_BT. The

large, positive energy barriers in Figure 4.7a can be used to effectively explain the near uninhibited transport of pnZVI through the low IS columns due to unfavorable, repulsive electrostatic conditions. However, for the 25 mmol IS, Figure 4.7b shows that there is a slightly larger repulsive barrier for the coated column, as compared to the uncoated column. Additionally, Figure 4.7b also shows a deeper secondary energy minimum for the uncoated column, as compared to the near zero secondary minimum for the coated column. Both of these results indicate that the highest pnZVI removal would be expected for the 25 mmol uncoated column configuration due to either overcoming the energy barrier to settle in the primary minimum by slow deposition, or through getting trapped in the secondary minimum by fast deposition. This result is not shown in the elution data, where the greatest retention of pnZVI occurs in the 25 mmol IS biofilm coated column, indicating that non-DLVO forces are likely responsible for the increased attachment efficiency.

Most importantly, in the context of this experiment, is that higher value of α for pnZVI in the 25 mmol biofilm covered column is not explained by DLVO energy considerations. As with the results of the T-E model, these results must be used cautiously due to the non-ideality of the system, evidenced by the incomplete coverage of biofilm on the collector surfaces (see Figure 5.1 below). Problems with the Hamaker constant discussed for the T-E model are compounded for the DLVO model due to the additional assumption that the collector zeta potential in the biofilm coated media is that of the bacteria for a given solution IS.

The assumed zeta potentials are likely incorrect, and probably could be

more negative and closer to that of the uncoated beads due to the incomplete coverage. However, an increase in zeta potential of the 25 mmol IS biofilm covered column would effectively increase the repulsive force between particle and collector, and therefore offer further evidence of the role of non-DLVO forces in the attachment process. It should also be considered that PAO1 biofilms are neutrally charged. As a result, the zeta potential of the biofilms may be reduced (less negative) as compared to the bacteria. In addition, even though biofilms have low coverage of bacteria on the glass media surfaces, there is likely a conditioning film on the media (Al-Bakri *et al.*, 2004) that could help neutralize the charge on the glass beads as well. The formation of these conditioning films are common in both natural and engineered aquatic systems, and can be formed due to the adsorption of dissolved organic matter or cell surface components. This may help explain the enhanced adhesion of biofilm bacteria, though non-DLVO forces likely impact nanoparticle transmission as well.

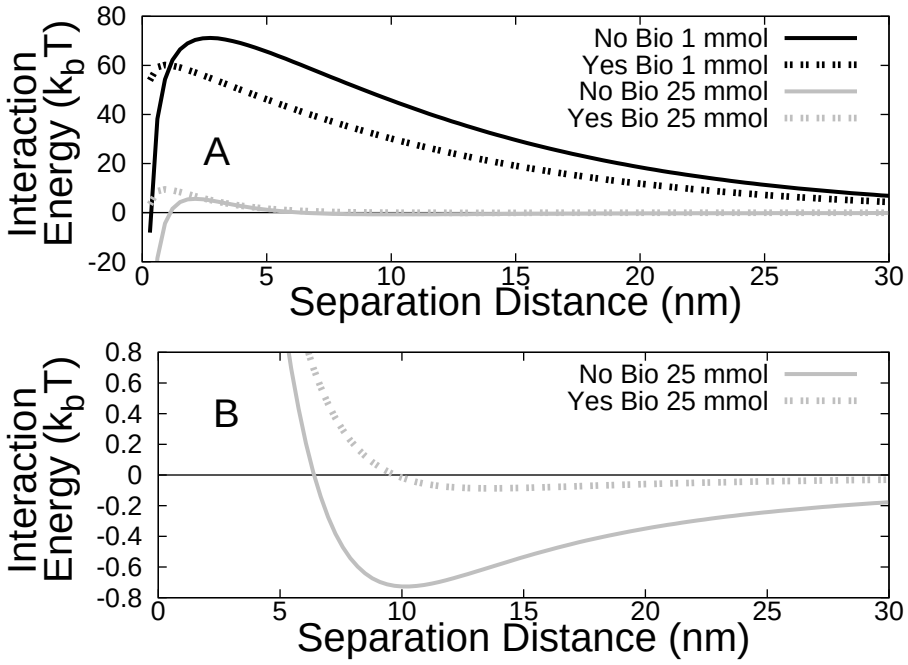

Figure 4.7: DLVO interaction energies in units of k_BT for the coated and uncoated columns, for both 1 and 25 mmol ISs. Panel a) illustrates the energy barrier to deposition, while b) shows the secondary minimum energy well.

Chapter 5

Discussion

The T-E model, in conjunction with DLVO theory, have been used to successfully explain particle filtration through saturated porous media (Tufenkji and Elimelech, 2005; Redman *et al.*, 2004). However, the results of this study indicate that with the addition of biofilm, the situation present in those studies does not occur, leading to incorrect predictions. In the context of snZVI transport, many studies have thus far relied on CFT to describe the transport effects of various surface modifications to nZVI (Saleh *et al.*, 2008; Kanel *et al.*, 2007; He *et al.*, 2009). Since snZVI is used for environmental remediation, it is necessarily going to be applied to natural systems that contain bacterial cell concentrations of the order of those present in this study. The only other published study of the effects of biofilm on the transport of engineered nanoparticles in saturated porous media also concluded that non-DLVO forces were responsible for increased particle filtration in the presence of biofilm (Tong *et al.*, 2010). Possible reasons for the increased retention of nanoparticles are discussed.

5.1 Physical Impacts of Biofilm Growth

Common theories in the literature point to surface charge heterogeneities (Tufenkji and Elimelech, 2005) or surface roughness (Shellenberger and Logan, 2002) to explain deviations observed from CFT. Figure 5.1 a and b, SEM images (Hitachi SEM S-2500) taken at magnifications of 150 and 500 times, respectively, show the incomplete coverage of biofilm on the glass beads, leading to surface charge heterogeneities, while Figure 5.1 b and c (12000 times magnification) illustrates the surface roughness inherent in the biofilm coated media.

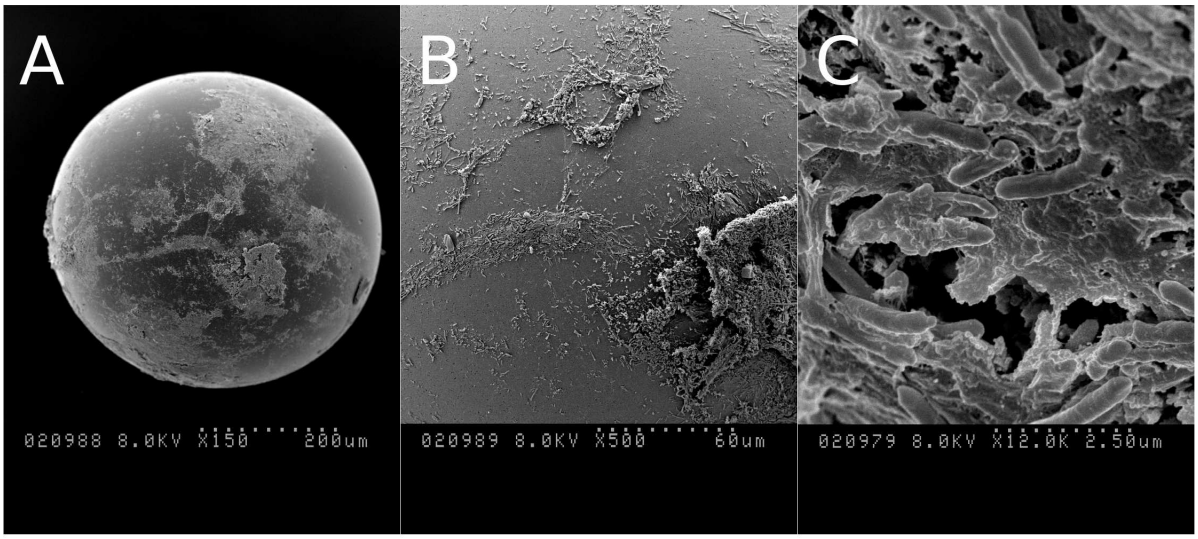

Figure 5.1: SEM images (Hitachi SEM S-2500) taken from a biofilm covered glass bead under a) 150 times b) 500 times and c) 12000 times magnification. The roughness and pore structure of the biofilm is illustrated.

The complex physical form of the biofilm could potentially lead to further sites of charge heterogeneity within the biofilm itself that could ultimately lead to locations with more favorable nanoparticle deposition, and hence an increase in the observed attachment efficiency. Additionally, the growth of

biofilm could constrict the available pore space of the porous media and lead to instances of particle removal by straining that are not predicted in CFT (Bradford *et al.*, 2006), or increase the turbulence of flow. Another physical feature of biofilm is its pore structure, as seen in Figure 5.1 c. Previous studies relating to the use of microbial granules in wastewater treatment have shown that a mechanism for the removal of 100 nm particles is through traversing into the pores of the biofilm (Ivanov *et al.*, 2004), which could also be occurring in this case.

None of these physical mechanisms are accounted for in CFT, but would not aid in explaining the results of this study due to the increased attachment measured only in the high IS biofilm coated column. Conversely, when compared to the low IS column, the higher IS would compress the biofilm EPS polymers and therefore decrease the surface roughness and turbulence, as well as potentially reduce the pore space lost to the biofilm.

The last physical consideration is the effects of the conditioning film on the glass beads. Conditioning films have been shown to increase bacterial adhesion to surfaces, with greater attachment measured with increasing IS (de Kerchove and Elimelech, 2007), and could similarly increase the attachment of nanoparticles.

5.2 Role of Other Forces

Physical impacts and DLVO forces have not been able to explain the results of this study, indicating that other forces, which are present only with increasing

IS, must be responsible.

The hydrophobicity of the system could potentially be responsible for the increased attachment measured at the high IS of the biofilm coated media. With increasing IS, pnZVI could come into closer contact with the biofilm and therefore be increasingly influenced by hydrophobic forces. However, due to limitations in the measurement of biofilm surface tensions, the impacts of hydrophobicity cannot be determined.

It has been shown, in the context of bacterial adhesion, that two like charged surfaces with polymer coatings (in this case the pnZVI and the EPS) could strongly bind by polymer bridging under conditions where the polymers protrude further than the EDL, and can therefore interact (Loosdrecht *et al.*, 1990). The bridging force can be used explain the results of this study due to the compression of the EDL only at the higher IS, as well as the presence of EPS polymers only in the biofilm coated column. This mechanism, however, does not explain the results of Tong *et al.* (2010), as the study was conducted using nanoparticles of C_{60} void of any surface polymers.

Another force that could explain these results is the steric force. At low IS, the anionic EPS is more stretched, and can therefore provide steric repulsion for the pnZVI. At the high IS, the conformation of these polymers is compressed (Frank and Belfort, 2003), lessening the magnitude of the steric force. This explanation encompasses the results measured in this study, as well as the results of Tong *et al.* (2010).

Chapter 6

Conclusions and Recommendations

CFT, even with DLVO energy considerations, is not adequate in describing, and therefore predicting the transport of pnZVI in the real subsurface environment due to the biological aspect of the soil matrix. Biofilm, being a complex aggregation of bacterial cells, as well as secreted EPS, is not well characterized by ideal single particle-collector interactions and the limitations of DLVO forces. The decreased steric force with the higher IS in the biofilm coated column is the likely contributor to the increased deposition measured in this experiment.

Furthermore, the importance of accurate models to predict transport distances of pnZVI in the real subsurface are needed in order to optimize contaminant remediation using these reactive nanoparticles, and to ensure that these particles are able to be delivered to contaminated zones. In future work, the

steric force, modeled by the Alexander de Gennes theory for polymer brushes (Kuhl *et al.*, 1994), should be considered, in combination with the DLVO model, to check for its ability in explaining the results obtained in this present experiment.

The results of this study indicate that caution should be used when employing CFT models for predicting the transport of snZVI in the environment. Additionally, the potential for a large variability in biofilm coverage of porous media, due to site specific environmental conditions, urges further discretion. Accordingly, future work should concentrate on comparing the impacts of biofilm composed of different bacterial species, or multiple species of bacteria, grown under various environmentally relevant conditions, on snZVI filtration.

The transport characteristics of different surface modifications of snZVI through biofilm coated systems should also be examined. Different surface coatings could potentially interact with biofilm coated media in unique ways that would not be elucidated in uncoated laboratory column tests. Thus, future experiments should test this hypothesis.

Finally, the results obtained in this study should be used to suggest that transport distances of snZVI in natural systems are likely overestimated by laboratory trials conducted with ideal, biofilm free porous media.

Bibliography

Al-Bakri, A., Gilbert, P. and Allison, D. (2004). Immigration and emigration of Burkholderia cepacia and Pseudomonas aeruginosa between and within mixed biofilm communities. *J. Appl. Microbiol.* 96, 455.

Alexander, M., Beamson, G., Blomfield, C., Leggett, G. and Duc, T. (2001). Interaction of carboxylic acids with the oxyhydroxide surface of aluminium: poly (acrylic acid), acetic acid and propionic acid on pseudoboehmite. *J. Electron Spectrosc. Relat. Phenom.* 121, 19.

Ambashta, R. and Sillanpaa, M. (2011). Experimental design of application of nanoscale iron-nickel under sonication and static magnetic field for mixed waste remediation. *J. Hazard. Mater.* Available online, doi:10.1016/j.jhazmat.2011.02.021.

Amir, A. and Lee, W. (2011). Enhanced reductive dechlorination of tetrachloroethene by nano-sized zero valent iron with vitamin B12. *Chem. Eng. J.* Available online, doi:10.1016/j.cej.2011.01.048.

AWWA (1992). *Standard methods for the examination of water and wastewater*. APHA Washington, DC.

Balkwill, D. and Ghiorse, W. (1985). Characterization of subsurface bacteria associated with two shallow aquifers in Oklahoma. *Appl. Environ. Microbiol.* 50, 580.

Bone, T. and Balkwill, D. (1988). Morphological and cultural comparison of microorganisms in surface soil and subsurface sediments at a pristine study site in Oklahoma. *Microb. Ecol.* 16, 49.

Bradford, S., Simunek, J., Bettahar, M., van Genuchten, M. and Yates, S. (2006). Significance of straining in colloid deposition: evidence and implications. *Water Resour. Res.* 42, W12S15.

Bradford, S. and Torkzaban, S. (2008). Colloid transport and retention in unsaturated porous media: a review of interface-, collector-, and pore-scale processes and models. *Vadose Zone J.* 7, 667.

Cantrell, K., Kaplan, D. and Wietsma, T. (1995). Zero-valent iron for the in situ remediation of selected metals in groundwater. *J. Hazard. Mater.* 42, 201.

Cao, J. and Zhang, W. (2006). Stabilization of chromium ore processing residue (COPR) with nanoscale iron particles. *J. Hazard. Mater.* 132, 213.

Chen, L., Yang, L., Zhao, X., Shen, L. and Duan, K. (2010). Identification of Pseudomonas aeruginosa genes associated with antibiotic susceptibility. *Sci. China, Ser. C: Life Sci.* 53, 1247.

Chen, S., Hsu, H. and Li, C. (2004). A new method to produce nanoscale iron for nitrate removal. *J. Nanopart. Res.* 6, 639.

Christensen, B. (1989). The role of extracellular polysaccharides in biofilms. *J. Biotechnol.* 10, 181.

Cosgrove, T. (2005). *Colloid science: principles, methods and applications.* Blackwell Publishing Limited.

Costerton, J., Cheng, K., Geesey, G., Ladd, T., Nickel, J., Dasgupta, M. and Marrie, T. (1987). Bacterial biofilms in nature and disease. *Annu. Rev. Microbiol.* 41, 435.

Costerton, J., Lewandowski, Z., Caldwell, D., Korber, D. and Lappin-Scott, H. (1995). Microbial biofilms. *Annu. Rev. Microbiol.* 49, 711.

Costerton, J., Stewart, P. and Greenberg, E. (1999). Bacterial biofilms: a common cause of persistent infections. *Science* 284, 1318.

Crabbe, A., Schurr, M., Monsieurs, P., Morici, L., Schurr, J., Wilson, J., Ott, C., Tsaprailis, G., Pierson, D. and Stefanyshyn-Piper, H. (2011). Transcriptional and proteomic responses of Pseudomonas aeruginosa PAO1 to spaceflight conditions involve Hfq regulation and reveal a role for oxygen. *Appl. Environ. Microbiol.* 77, 1221.

Czupyrna, G., Levy, R., MacLean, A. and Gold, H. (1992). In situ immobilization of heavy metal-contaminated soils. *J. Soil Sci.* 154, 338.

de Kerchove, A. and Elimelech, M. (2007). Impact of alginate conditioning film on deposition kinetics of motile and nonmotile Pseudomonas aeruginosa strains. *Appl. Environ. Microbiol.* 73, 5227.

Derjaguin, B. and Landau, L. (1941). Theory of stability of highly charged lyophobic sols and adhesion of highly charged particles in solutions of electrolytes. *Acta Physicochim. URSS* 14, 633.

Donlan, R. (2001). Biofilm formation: a clinically relevant microbiological process. *Clin. Infect. Dis.* 33, 1387.

Doyle, M. (2006). *Nanotechnology: a brief literature review*. Food Research Institute, UW-Madison.

Einstein, A. (1905). Uber einen die Erzeugung und Verwandlung des Lichtes betreffenden heuristischen Gesichtspunkt. *Ann. Phys.* 322, 132.

Fatisson, J., Ghoshal, S. and Tufenkji, N. (2010). Deposition of carboxymethylcellulose-coated zero-valent iron nanoparticles onto silica: roles of solution chemistry and organic molecules. *Langmuir* 26, 12832.

Franco, D., Da Silva, L. and Jardim, W. (2009). Reduction of hexavalent chromium in soil and ground water using zero-valent iron under batch and semi-batch conditions. *Water Air Soil Pollut.* 197, 49.

Frank, B. and Belfort, G. (2003). Polysaccharides and sticky membrane surfaces: critical ionic effects. *J. Membr. Sci.* 212, 205.

Gillham, R. and O'Hannesin, S. (1994). Enhanced degradation of halogenated aliphatics by zero-valent iron. *Ground Water* 32, 958.

Gregory, J. (1981). Approximate expressions for retarded van der Waals interaction. *J. Colloid Interface Sci.* 83, 138.

Hall-Stoodley, L. and Stoodley, P. (2005). Biofilm formation and dispersal and the transmission of human pathogens. *Trends Microbiol.* 13, 7.

Happel, J. (1958). Viscous flow in multiparticle systems: slow motion of fluids relative to beds of spherical particles. *AIChE J.* 4, 197.

Hardalo, C. and Edberg, S. (1997). Pseudomonas aeruginosa: assessment of risk from drinking water. *Crit. Rev. Microbiol.* 23, 47.

He, F., Zhang, M., Qian, T. and Zhao, D. (2009). Transport of carboxymethyl cellulose stabilized iron nanoparticles in porous media: column experiments and modeling. *J. Colloid Interface Sci.* 334, 96.

He, F. and Zhao, D. (2005). Preparation and characterization of a new class of starch-stabilized bimetallic nanoparticles for degradation of chlorinated hydrocarbons in water. *Environ. Sci. Technol.* 39, 3314.

He, F., Zhao, D., Liu, J. and Roberts, C. (2007). Stabilization of Fe-Pd nanoparticles with sodium carboxymethyl cellulose for enhanced transport and dechlorination of trichloroethylene in soil and groundwater. *Ind. Eng. Chem. Res.* 46, 29.

Holmberg, K. (2002). *Handbook of applied surface and colloid chemistry.* John Wiley.

Hunter, R., Phoenix, V., Saxena, A. and Beveridge, T. (2010). Impact of growth environment and physiological state on metal immobilization by Pseudomonas aeruginosa PAO1. *Can. J. Microbiol.* 56, 527.

Hydutsky, B., Mack, E., Beckerman, B., Skluzacek, J. and Mallouk, T. (2007). Optimization of nano-and microiron transport through sand columns using polyelectrolyte mixtures. *Environ. Sci. Technol* 41, 6418.

Israelachvili, J. (1992). *Intermolecular and surface forces*. Academic press London.

Ivanov, V., Tay, J., Tay, S. and Jiang, H. (2004). Removal of micro-particles by microbial granules used for aerobic wastewater treatment. *Water Sci. Technol.* 50, 147.

Kadar, E., Tarran, G., Jha, A. and Al-Subiai, S. (2011). Stabilization of engineered zero-valent nanoiron with Na-acrylic copolymer enhances spermiotoxicity. *Environ. Sci. Technol.* Available online, doi:10.1021/es1029848.

Kanel, S., Clement, T., Barnett, M. and Goltz, M. (2011). Nano-scale hydroxyapatite: synthesis, two-dimensional transport experiments, and application for uranium remediation. *J. Nanotechnol.* 21, 22.

Kanel, S., Nepal, D., Manning, B. and Choi, H. (2007). Transport of surface-modified iron nanoparticle in porous media and application to arsenic (III) remediation. *J. Nanopart. Res.* 9, 725.

Klimkova, S., Cernik, M., Lacinova, L., Filip, J., Jancik, D. and Zboril, R. (2011). Zero-valent iron nanoparticles in treatment of acid mine water from in situ uranium leaching. *Chemosphere* 8, 1178.

Klockgether, J., Munder, A., Neugebauer, J., Davenport, C., Stanke, F., Larbig, K., Heeb, S., Schock, U., Pohl, T. and Wiehlmann, L. (2010). Genome diversity of Pseudomonas aeruginosa PAO1 laboratory strains. *J. Bacteriol.* 192, 1113.

Korber, D., Lawrence, J., Sutton, B. and Caldwell, D. (1989). Effect of laminar flow velocity on the kinetics of surface recolonization by Mot+ and Mot- Pseudomonas fluorescens. *Microb. Ecol.* 18, 1.

Kuhl, T., Leckband, D., Lasic, D. and Israelachvili, J. (1994). Modulation of interaction forces between bilayers exposing short-chained ethylene oxide headgroups. *Biophys. J.* 66, 1479.

Leadley, S. and Watts, J. (1997). The use of XPS to examine the interaction of poly (acrylic acid) with oxidised metal substrates. *J. Electron Spectrosc. Relat. Phenom.* 85, 107.

Lecoanet, H. and Wiesner, M. (2004). Velocity effects on fullerene and oxide nanoparticle deposition in porous media. *Environ. Sci. Technol.* 38, 4377.

Li, J., McLellan, S. and Ogawa, S. (2006). Accumulation and fate of green fluorescent labeled Escherichia coli in laboratory-scale drinking water biofilters. *Water Research* 40, 3023.

Li, X., Cao, J. and Zhang, W. (2008). Stoichiometry of Cr (VI) immobilization using nanoscale zerovalent iron (nZVI): a study with high-resolution X-ray photoelectron spectroscopy (HR-XPS). *Ind. Eng. Chem. Res.* 47, 2131.

Lin, Y., Tseng, H., Wey, M. and Lin, M. (2010). Characteristics of two types of stabilized nano zero-valent iron and transport in porous media. *Sci. Total Environ.* 408, 2260.

Liu, Y. and Li, J. (2008). Role of Pseudomonas aeruginosa biofilm in the initial adhesion, growth and detachment of Escherichia coli in porous media. *Environ. Sci. Technol.* 42, 443.

Liu, Y., Yang, C. and Li, J. (2007). Influence of extracellular polymeric substances on Pseudomonas aeruginosa transport and deposition profiles in porous media. *Environ. Sci. Technol* 41, 198.

Lo, I., Lam, C. and Lai, K. (2006). Hardness and carbonate effects on the reactivity of zero-valent iron for Cr (VI) removal. *Water Res.* 40, 595.

Loosdrecht, M., Norde, W., Lyklema, J. and Zehnder, A. (1990). Hydrophobic and electrostatic parameters in bacterial adhesion. *Aquat. Sci.* 52, 103.

Lowry, G. and Johnson, K. (2004). Congener-specific dechlorination of dissolved PCBs by microscale and nanoscale zerovalent iron in a water/methanol solution. *Environ. Sci. Technol.* 38, 5208.

Norris, G., Al-Dhahir, Z., Birnstingl, J., Plant, S., Cui, S. and Mayell, P. (1999). A case study of the management and remediation of soil contaminated with polychlorinated biphenyls. *Eng. Geol.* 53, 177.

Nyer, E. and Vance, D. (2001). Nano-scale iron for dehalogenation. *Ground Water Monit. Rem.* 21, 41.

Oste, L., Lexmond, T. and Van Riemsdijk, W. (2002). Metal immobilization in soils using synthetic zeolites. *J. Environ. Qual.* 31, 813.

Pardieck, D., Bouwer, E. and Stone, A. (1992). Hydrogen peroxide use to increase oxidant capacity for in situ bioremediation of contaminated soils and aquifers: a review. *J. Contam. Hydrol.* 9, 221.

Pelley, A. and Tufenkji, N. (2008). Effect of particle size and natural organic matter on the migration of nano-and microscale latex particles in saturated porous media. *J. Colloid Interface Sci.* 321, 74.

Ponder, S., Darab, J. and Mallouk, T. (2000). Remediation of Cr (VI) and Pb (II) aqueous solutions using supported, nanoscale zero-valent iron. *Environ. Sci. Technol.* 34, 2564.

Puls, R., Paul, C. and Powell, R. (1999). The application of in situ permeable reactive (zero-valent iron) barrier technology for the remediation of chromate-contaminated groundwater: a field test. *Appl. Geochem.* 14, 989.

Quinn, J., Geiger, C., Clausen, C., Brooks, K., Coon, C., O'Hara, S., Krug, T., Major, D., Yoon, W., Gavaskar, A. and Holdsworth, T. (2005). Field demonstration of DNAPL dehalogenation using emulsified zero-valent iron. *Environ. Sci. Technol.* 39, 1309.

Rajagopalan, R. and Tien, C. (1976). Trajectory analysis of deep-bed filtration with the sphere-in-cell porous media model. *AIChE J.* 22, 523.

Redman, J., Walker, S. and Elimelech, M. (2004). Bacterial adhesion and

transport in porous media: role of the secondary energy minimum. *Environ. Sci. Technol.* 38, 1777.

Rosenberg, M., Bayer, E., Delarea, J. and Rosenberg, E. (1982). Role of thin fimbriae in adherence and growth of Acinetobacter calcoaceticus RAG-1 on hexadecane. *Appl. Environ. Microbiol.* 44, 929.

Saleh, N., Kim, H., Phenrat, T., Matyjaszewski, K., Tilton, R. and Lowry, G. (2008). Ionic strength and composition affect the mobility of surface-modified Fe0 nanoparticles in water-saturated sand columns. *Environ. Sci. Technol.* 42, 3349.

Saleh, N., Sirk, K., Liu, Y., Phenrat, T., Dufour, B., Matyjaszewski, K., Tilton, R. and Lowry, G. (2007). Surface modifications enhance nanoiron transport and NAPL targeting in saturated porous media. *Environ. Eng. Sci.* 24, 45.

Sarathy, V., Salter, A., Nurmi, J., O'Brien Johnson, G., Johnson, R. and Tratnyek, P. (2009). Degradation of 1, 2, 3-trichloropropane (TCP): hydrolysis, elimination, and reduction by iron and zinc. *Environ. Sci. Technol.* 44, 787.

Satapanajaru, T., Anurakpongsatorn, P., Pengthamkeerati, P. and Boparai, H. (2008). Remediation of atrazine-contaminated soil and water by nano zerovalent iron. *Water Air Soil Pollut.* 192, 349.

Schrick, B., Hydutsky, B., Blough, J. and Mallouk, T. (2004). Delivery vehicles for zerovalent metal nanoparticles in soil and groundwater. *Chem. Mater.* 16, 2187.

Seaman, J., Bertsch, P. and Schwallie, L. (1999). In situ Cr (VI) reduction within coarse-textured, oxide-coated soil and aquifer systems using Fe (II) solutions. *Environ. Sci. Technol.* 33, 938.

Senzaki, T. (1991). Removal of chlorinated organic compounds from wastewater by reduction process: III. Treatment of trichloroethylene with iron powder. *Kogyo Yosui* 391, 29.

Senzaki, T. and Kumagai, Y. (1988). Treatment of 1, 1, 2, 2-Tetrachloroethane with iron powder. *Kogyo Yosui* 357, 2.

Senzaki, T. and Kumagai, Y. (1989). Removal of chlorinated organic compounds from wastewater by reduction process: II. Treatment of trichloroethylene with iron powder. *Kogyo Yosui* 369, 19.

Shellenberger, K. and Logan, B. (2002). Effect of molecular scale roughness of glass beads on colloidal and bacterial deposition. *Environ. Sci. Technol.* 36, 184.

Smith, R. and Iglewski, B. (2003). P. aeruginosa quorum-sensing systems and virulence. *Curr. Opin. Microbiol.* 6, 56.

State of California (2005). *Waste extraction test (WET) procedures*. State of California. Available at: www.dtsc.ca.gov/LawsRegsPolicies/Title22/upload/OEARA_REG_Title22_Ch11_AppII.pdf [accessed 8 March 2011].

Stover, C., Pham, X., Erwin, A., Mizoguchi, S., Warrener, P., Hickey, M., Brinkman, F., Hufnagle, W., Kowalik, D. and Lagrou, M. (2000). Com-

plete genome sequence of Pseudomonas aeruginosa PA01, an opportunistic pathogen. *Nature* 406, 959.

Su, C. and Puls, R. (2003). In situ remediation of arsenic in simulated groundwater using zerovalent iron: laboratory column tests on combined effects of phosphate and silicate. *Environ. Sci. Technol.* 37, 2582.

Takase, H. (2009). Influence of interparticle forces on selective wet agglomeration. *Adv. Powder Technol.* 20, 327.

Tiraferri, A. and Sethi, R. (2009). Enhanced transport of zerovalent iron nanoparticles in saturated porous media by guar gum. *J. Nanopart. Res.* 11, 635.

Tong, M., Ding, J., Shen, Y. and Zhu, P. (2010). Influence of biofilm on the transport of fullerene (C60) nanoparticles in porous media. *Water Research* 44, 1094.

Triandafillu, K., Balazs, D., Aronsson, B., Descouts, P., Tu Quoc, P., van Delden, C., Mathieu, H. and Harms, H. (2003). Adhesion of Pseudomonas aeruginosa strains to untreated and oxygen-plasma treated poly (vinyl chloride)(PVC) from endotracheal intubation devices. *Biomaterials* 24, 1507.

Tufenkji, N. and Elimelech, M. (2004a). Correlation equation for predicting single-collector efficiency in physicochemical filtration in saturated porous media. *Environ. Sci. Technol.* 38, 529.

Tufenkji, N. and Elimelech, M. (2004b). Deviation from the classical colloid

filtration theory in the presence of repulsive DLVO interactions. *Langmuir* 20, 10818.

Tufenkji, N. and Elimelech, M. (2005). Breakdown of colloid filtration theory: role of the secondary energy minimum and surface charge heterogeneities. *Langmuir* 21, 841.

U.S. EPA (1998a). *Toxicological review of hexavalent chromium.* Washington, DC: Environmental Protection Agency. Available at: www.epa.gov/iris/toxreviews/0144tr.pdf [accessed 8 March 2011].

U.S. EPA (1998b). *Toxicological review of trivalent chromium.* Washington, DC: Environmental Protection Agency. Available at: www.epa.gov/iris/toxreviews/0028tr.pdf [accessed 8 March 2011].

U.S. EPA (2000). *Hudson River PCBs Superfund site.* Washington, DC: Environmental Protection Agency. Available at: www.epa.gov/hudson/proposedplan.pdf [accessed 8 March 2011].

U.S. EPA (2003). *Method 1311: toxicity characteristic leaching procedure.* Washington, DC: Environmental Protection Agency. Available at: www.epa.gov/osw/hazard/testmethods/sw846/pdfs/1311.pdf [accessed 8 March 2011].

Varanasi, P., Fullana, A. and Sidhu, S. (2007). Remediation of PCB contaminated soils using iron nano-particles. *Chemosphere* 66, 1031.

Verwey, E. (1947). Theory of the stability of lyophobic colloids. *J. Phys. Colloid Chem.* 51, 631.

Waldvogel, F. and Bisno, A. (2000). *Infections associated with indwelling medical devices*. ASM Press Washington DC.

Wang, C. and Zhang, W. (1997). Synthesizing nanoscale iron particles for rapid and complete dechlorination of TCE and PCBs. *Environ. Sci. Technol.* 31, 2154.

Watnick, P. and Kolter, R. (2000). Biofilm, city of microbes. *J. Bacteriol.* 182, 2675.

Webster, J., Hampton, G., Wilson, J., Ghiorse, W. and Leach, F. (1985). Determination of microbial cell numbers in subsurface samples. *Ground Water* 23, 17.

Wilson, J., McNabb, J., Balkwill, D. and Ghiorse, W. (1983). Enumeration and characterization of bacteria indigenous to a shallow water-table aquifer. *Ground Water* 21, 134.

Wozniak, D., Wyckoff, T., Starkey, M., Keyser, R., Azadi, P., O'Toole, G. and Parsek, M. (2003). Alginate is not a significant component of the extracellular polysaccharide matrix of PA14 and PAO1 Pseudomonas aeruginosa biofilms. *Proc. Natl. Acad. Sci. U. S. A.* 100, 7907.

Xu, Y. and Zhao, D. (2007). Reductive immobilization of chromate in water and soil using stabilized iron nanoparticles. *Water Research* 41, 2101.

Yang, G., Tu, H. and Hung, C. (2007). Stability of nanoiron slurries and their transport in the subsurface environment. *Sep. Purif. Technol.* 58, 166.

Yao, K., Habibian, M. and O'Melia, C. (1971). Water and waste water filtration. Concepts and applications. *Environ. Sci. Technol.* 5, 1105.

Yoon, S., Hennigan, R., Hilliard, G., Ochsner, U., Parvatiyar, K., Kamani, M., Allen, H., DeKievit, T., Gardner, P., Schwab, U. *et al.* (2002). Pseudomonas aeruginosa anaerobic respiration in biofilms: relationships to cystic fibrosis pathogenesis. *Dev. Cell* 3, 593.

Zhang, J. and Li, X. (1987). Chromium pollution of soil and water in Jinzhou. *Zhonghua yu fang yi xue za zhi [Chi. J. Prev. Med.]* 21, 262.

Zhang, W. (2003). Nanoscale iron particles for environmental remediation: an overview. *J. Nanopart. Res.* 5, 323.

Zhang, W., Wang, C. and Lien, H. (1998). Treatment of chlorinated organic contaminants with nanoscale bimetallic particles. *Catal. Today* 40, 387.

Zhang, X. and Bishop, P. (2003). Biodegradability of biofilm extracellular polymeric substances. *Chemosphere* 50, 63.